Intranasal Immunization with a Lentiviral Vector Coding for SARS-CoV-2 Spike Protein Confers Vigorous Protection in Pre-Clinical Animal Models

Abstract

We developed a potent vaccination strategy, based on lentiviral vector (LV), capable of inducing neutralizing antibodies specific to the Spike glycoprotein (S) of SARS-CoV-2, the etiologic agent of CoronaVirus Disease 2019 (COVID-19). Among several LV encoding distinct variants of S, a single one encoding the full-length, membrane anchored S (LV::S_{FL}) triggered high antibody titers in mice, with neutralization activities comparable to patients recovered from COVID-19. LV::S_{FL} systemic vaccination in mice, in which the expression of the CoV2 receptor hACE2 was induced by transduction of the respiratory tract cells by an adenoviral type 5 (Ad5) vector, despite an intense serum neutralizing activity, only ≈1 $\log_{10}$ reduction of lung viral loads was observed after SARS-CoV2 challenge.

We thus explored the strategy of targeting the immune response to the upper respiratory tract through an intranasal boost administration. Even though, after a prime and target regimen, the systemic neutralizing activity did not increase substantially, ≈5 $\log_{10}$ decrease in lung viral loads was achieved, with the loads in some animals under the limit of detection of a highly sensitive RT-PCR assay. The conferred protection also avoided largely pulmonary inflammation. We confirmed the vaccine efficacy and inhibition of lung inflammation using both integrative and non-integrative LV platforms in golden hamsters, naturally permissive to SARS-CoV2 replication and restituting human COVID-19 physiopathology. Our results provide the proof-of-principle evidence of marked prophylactic effects of an LV-based vaccination strategy against SARS-CoV-2 in two pre-clinical animal models and designate the intranasal LV::S_{FL}-based immunization as a vigorous and promising vaccine approach against COVID-19.

Intranasal Immunization with a Lentiviral Vector Coding for SARS-CoV-2 Spike Protein Confers Vigorous Protection in Pre-Clinical Animal Models

Min-Wen Ku[1*], Maryline Bourgine[1,2*], Pierre Authié[1*], Jodie Lopez[1], Kirill Nemirov[1], Fanny Moncoq[1], Amandine Noirat[1], Benjamin Vesin[1], Fabien Nevo[1], Catherine Blanc[1], Philippe Souque[2], Emeline Simon[3], Houda Tabbal[3], Hugo Mouquet[4], François Anna[1], Annette Martin[3], Nicolas Escriou[5], Laleh Majlessi[1£] and Pierre Charneau[1,2£]

[1]Institut Pasteur-TheraVectys Joint Lab, 28 rue du Dr. Roux, Paris F-75015, France

[2]Molecular Virology and Vaccinology Unit, Institut Pasteur

[3]Molecular Genetics of RNA Viruses Unit, Institut Pasteur. CNRS UMR3569, Université Paris Diderot-Sorbonne, Paris Cité, Paris, France

[4]Laboratory of Humoral Immunology, Institut Pasteur, INSERM U1222

[5]Innovation Lab, Vaccines, Institut Pasteur

[*]Equal contribution of the authors

[£]Co-senior and co-corresponding authors

Abstract

We developed a potent vaccination strategy, based on lentiviral vector (LV), capable of inducing neutralizing antibodies specific to the Spike glycoprotein (S) of SARS-CoV-2, the etiologic agent of CoronaVirus Disease 2019 (COVID-19). Among several LV encoding distinct variants of S, a single one encoding the full-length, membrane anchored S (LV::S_{FL}) triggered high antibody titers in mice, with neutralization activities comparable to patients recovered from COVID-19. LV::S_{FL} systemic vaccination in mice, in which the expression of the CoV2 receptor hACE2 was induced by transduction of the respiratory tract cells by an adenoviral type 5 (Ad5) vector, despite an intense serum neutralizing activity, only ≈1 $\log_{10}$ reduction of lung viral loads was observed after SARS-CoV2 challenge.

We thus explored the strategy of targeting the immune response to the upper respiratory tract through an intranasal boost administration. Even though, after a prime and target regimen, the systemic neutralizing activity did not increase substantially, ≈5 $\log_{10}$ decrease in lung viral loads was achieved, with the loads in some animals under the limit of detection of a highly sensitive RT-PCR assay. The conferred protection also avoided largely pulmonary inflammation.

We confirmed the vaccine efficacy and inhibition of lung inflammation using both integrative and non-integrative LV platforms in golden hamsters, naturally permissive to SARS-CoV2 replication and restituting human COVID-19 physiopathology. Our results provide the proof-of-principle evidence of marked prophylactic effects of an LV-based vaccination strategy against SARS-CoV-2 in two pre-clinical animal models and designate the intranasal LV::S_{FL}-based immunization as a vigorous and promising vaccine approach against COVID-19.

Introduction

The new Severe Acute Respiratory Syndrome beta-coronavirus 2 (SARS-CoV-2) that emerged in late 2019 in Wuhan, China, is extraordinarily contagious and fast-spreading across the world (Guo et al., 2020). Compared to the previously emerged SARS or Middle East Respiratory Syndrome (MERS) coronaviruses, SARS-CoV-2 causes unprecedented threat on global health and tremendous socio-economic consequences. Therefore, the development of effective prophylactic vaccines against SARS-CoV-2 is an absolute imperative to contain the spread of the epidemic and to attenuate the onset of CoronaVirus Disease 2019 (COVID-19), such as deleterious inflammation and progressive respiratory failure (Amanat and Krammer, 2020).

Coronaviruses are enveloped, non-segmented positive-stranded RNA viruses, characterized by their envelope-anchored Spike (S) glycoprotein (Walls et al., 2020). The SARS-CoV-2 S (S_{CoV-2}) is a $(180\ kDa)_3$ homotrimeric class I viral fusion protein, that engages the carboxypeptidase Angiotensin-Converting Enzyme 2 (ACE2), expressed on host cells. The monomer of S_{CoV-2} protein possesses an ecto-domain, a transmembrane anchor domain, and a short internal tail. S_{CoV-2} is activated by a two-step sequential proteolytic cleavage to initiate fusion with the host cell membrane. Subsequent to S_{CoV-2}-ACE2 interaction, through a conformational reorganization, the extracellular domain of S_{CoV-2} is first cleaved at the highly specific furin $682^{RRAR}685$ site (Guo et al., 2020; Walls et al., 2020), a key factor determining the pathological features of the virus, linked to the ubiquitous furin expression (Wang et al., 2020). The resulted subunits are constituted of: (i) S1, which harbors the ACE2 Receptor Binding Domain (RBD), with the atomic contacts restricted to the ACE2 protease domain, and (ii) S2, which bears the membrane-fusion elements. Like for S_{CoV-1}, the shedding of S1 renders accessible on S2 the second proteolytic cleavage site 797^{R}, namely S2' (Belouzard et al., 2009). According to the cell or tissue types, one or several host proteases, including furin, trypsin, cathepsins or transmembrane protease serine protease-2 or -4, can be involved in this second cleavage step (Coutard et al., 2020). The consequent "fusogenic" conformational changes of S lead to the exposure of a Fusion Peptide (FP), adjacent to S2'. Insertion of FP to the host cell/vesicle membrane primes the fusion reaction, whereby the viral RNA release into the host cytosol (Lai et al., 2017). The facts that the S_{CoV-2}-ACE2 interaction is the only mechanism, thus far identified for the host cell infection by SARS-CoV-2, and that the RBD contains numerous conformational B-cell epitopes (Walls et al., 2020), designate this viral envelope glycoprotein as the main target for neutralizing antibodies (nAbs).

Compared to: (i) attenuated or inactivated viral vaccine candidates which require extensive safety testing, (ii) nucleic acid encoding for S without proven efficacy, (iii) protein vaccines which require the use of adjuvants and boosting, viral vector vaccines, such as adenoviral vectors, can generate strong immune response. However, adenoviral vectors are target of pre-existing immunity in the human population, which largely reduces their immunogenicity (Rosenberg et al., 1998; Schirmbeck et al.,

75 2008). Non-replicative lentiviral vaccinal vectors (LV) possess a large potential at eliciting strong and
76 long-lasting adaptive immunity, including Ab responses (Di Nunzio et al., 2012; Hu et al., 2011; Ku et
77 al., 2020; Zennou et al., 2000). The safety of these vectors has been demonstrated in human in a phase
78 1 HIV-1 vaccine trial (2011-006260-52 EN). In addition, LV are majorly pseudo-typed with Vesicular
79 Stomatitis Virus envelope Glycoprotein (VSV-G), with negligible exposure in human population,
80 which minimizes the risk of vaccine efficacy reduction linked to a pre-existing cross-reactive immunity
81 as described for other viral vectors (Hu et al., 2011).

82 To develop a vaccine candidate able to induce nAbs specific to S_{CoV-2}, we generated LV coding for:
83 (i) full-length, membrane anchored form of S (LV::S_{FL}), (ii) S1-S2 ecto-domain, without the
84 transmembrane and internal tail domains (LV::S1-S2), or (iii) S1 alone (LV::S1). We established that
85 LV::S_{FL} gave rise to elevated amounts of nAbs, inhibiting the $ACE2^+$ host-cell invasion by S_{CoV-2}-
86 pseudo-typed virions. S_{CoV-2}-specific T cells were also efficaciously induced in LV::S_{FL}-immunized
87 animals. Moreover, in a mouse model in which the expression of human ACE2 (hACE2) was induced
88 in the respiratory tracts by an adenoviral vector serotype 5 (Ad5), as well as in golden hamsters, we
89 demonstrated a strong prophylactic effect of LV::S_{FL} immunization against the replication of a SARS-
90 CoV-2 clinical isolate, accompanied by the reduction of infection-related inflammation in the lungs.
91 Importantly, boost/target immunization with LV::S_{FL} via nasal route was instrumental in the protection
92 efficacy. Our virological and immunological criteria provided the proof-of-principle evidence of: (i)
93 marked prophylactic effects of a viral vector-based vaccination strategy against SARS-CoV-2, (ii) the
94 fact that LV-based immunization represents a promising strategy to develop vaccine candidates against
95 coronaviruses, and (iii) requirement of mucosal immunization to reach vigorous protective lung
96 immunity.

97 **Results**

98 **Induction of antibody responses by LV encoding SARS-CoV-2 Spike protein variants**

99 To develop a vaccine candidate able to induce nAbs specific to S_{CoV-2}, we generated LV coding,
100 under the transcriptional control of the cytomegalovirus (CMV) immediate-early promoter, for codon-
101 optimized sequences of: (i) full-length, membrane anchored form of S (LV::S_{FL}), (ii) S1-S2 ecto-
102 domain, without the transmembrane and C-terminal short internal tail (LV::S1-S2), or (iii) S1 alone
103 (LV::S1), which all harbor the RBD **(Figure 1A, Supplemental Figure 1)**, with prospective
104 conformational heterogeneities. To evaluate the humoral responses induced by these vectors, C57BL/6
105 mice (n = 4/group) were immunized by a single i.p. injection of 1×10^7 TU/mouse of either LV, or an
106 LV encoding GFP as negative control. S_{CoV-2}-specific Ab responses were investigated in the sera at
107 weeks 1, 2, 3, 4 and 6 post immunization **(Figure 1B)**. In LV::S_{FL} or LV::S1-S2-immunized mice,
108 S_{CoV-2}-specific immunoglobulin G (IgG) were detectable as early as 1 week post immunization and
109 their amounts exhibited a progressive increment until week 6 post immunization with Mean titer ±
110 SEM of $(4.5 \pm 2.9) \times 10^6$ or $(1.5 \pm 1) \times 10^6$, respectively. In comparison, S_{CoV-2}-specific IgG titers were
111 100× lower, i.e., $(7.1 \pm 6.1) \times 10^4$, in their LV::S1-immunized counterparts.

112 Sera were then evaluated for their capacity to neutralize SARS-CoV-2, using a reliable
113 neutralization assay based on nAb-mediated inhibition of $hACE2^+$ cell invasion by non-replicative LV
114 particle surrogates, pseudo-typed with S_{CoV-2} (Sterlin et al.). Such S_{CoV-2} pseudo-typed LV particles,
115 harbor the reporter luciferase gene, which allows quantitation of the $hACE2^+$ host cell invasion,
116 inversely proportional to the neutralization efficiency of nAbs possibly contained in the biological
117 fluids. Analysis of 50% Effective Concentrations (EC50) of the sera from the LV::S_{FL}-, LV::S1-S2- or
118 LV::S1-immunized mice clearly established that LV::S_{FL} was the most potent vector at inducing S_{CoV-}
119 $_{2}$-specific nAbs **(Figure 1C)**. Moreover, nAb titers were correlated with S_{CoV-2}-specific IgG titers only
120 in the sera of LV::S_{FL}-immunized mice ($p < 0.0001$, $R^2 = 0.645$, two-sided Spearman rank-correlation
121 test) **(Figure 1D)**. These results strongly suggest that in the S1-S2 or S1 polypeptides, the
122 conformations of pertinent B-cell epitopes are distinct from those of the native S_{FL}, the latter
123 representing the only variant which induces nAbs able to inhibit the S_{CoV-2}-hACE2 interaction and host
124 cell invasion. Comparison of the neutralizing capacity of sera from the LV::S_{FL}-immunized mice and
125 a cohort of mildly symptomatic infected people living in Crépy en Valois, one of the first epidemic
126 zones appeared in France, showed equivalent neutralizing activity average **(Figure 1E)**. These data
127 predict a potentially protective humoral response induced by LV::S_{FL}.

128 LV::S_{FL}-immunized C57BL/6 mice also displayed S_{CoV-2}-specific T-cell responses, as detected at
129 week 2 post-immunization by IFNγ ELISPOT assay following stimulation with distinct pools of S_{CoV-}
130 $_{2}$-derived 15-mer peptides, spanning the S_{FL} **(Figure 2A)**. Significant amounts of responding T cells
131 were detected for 4 out of 10 peptide pools. Deconvolution of the 4 positive pools by intracellular

132 cytokine staining detected at least one immunogenic region able to stimulate $CD4^+$ T cells (**Figure 2B,**
133 right panel) versus 4 regions able to stimulate $CD8^+$ T cells (**Figure 2B,** left panel), which is in
134 accordance with the favored orientation of LV-encoded antigens to the MHC-I presentation pathway
135 (Hu et al., 2011).

136 **Set up of a murine model expressing human ACE2 in the respiratory tracts**

137 As S_{CoV-2} does not interact well with murine ACE2, wild-type laboratory mice are not permissive to
138 replication of SARS-CoV-2 clinical isolates. Due to unavailability of hACE2 transgenic mice in
139 Europe during the progression of the present study, we sought to elaborate a murine model in which
140 the hACE2 expression is induced in the respiratory tracts and pulmonary mucosa to evaluate the
141 LV::S_{FL} vaccine efficacy. We generated an Ad5 gene delivery vector able to vehicle in non-integrating
142 episomes, the gene coding for hACE2 under the transcriptional control of CMV promoter
143 (Ad5::hACE2). We first checked in vitro the potential of the Ad5::hACE2 vector to transduce
144 HEK293T cells by RT-PCR **(Figure 3A)**. To achieve in vivo transduction of respiratory tract cells, we
145 instilled i.n. 2.5×10^9 IGU/mouse of Ad5::hACE2 into C57BL/6 mice. Four days later, the hACE2
146 protein expression was detectable in the lung cell homogenate by Western Blot **(Figure 3B)**. To get
147 more insights into the in vivo expression profile of a transgene administered under these conditions,
148 we instilled i.n. the same dose of an Ad5::GFP reporter vector into C57BL/6 mice. As evaluated by
149 flow cytometry, 4 days post instillation, the GFP reporter was expressed not only in the lung epithelial
150 $EpCam^+$ cells, but also in lung immune cells, as tracked by CD45 pan-hematopoietic marker **(Figure**
151 **3C)**, showing that this approach allows efficient transduction of epithelial cells which however is not
152 restricted to these cells.

153 To evaluate the permissibility of such hACE2-transduced mice to SARS-CoV-2 infection, 4 days
154 after i.n. pretreatment with either Ad5::hACE2 or an empty control Ad5 vector, C57BL/6 mice were
155 inoculated i.n. with 1×10^5 $TCID_{50}$ of a SARS-CoV-2 clinical isolate, which was isolated in February
156 2020 from a COVID-19 patient by the National Reference Centre for Respiratory Viruses (Institut
157 Pasteur, France). The lung viral loads, determined at 2 days post inoculation (dpi), were as high as (4.4
158 $\pm$ 1.8) $\times 10^9$ copies of SARS-CoV-2 RNA/mouse in Ad5::hACE2-pretreated mice, compared to only
159 (6.2 $\pm$ 0.5) $\times 10^5$ copies/mouse in empty Ad5-pretreated, or (4.0 $\pm$ 2.9) $\times 10^5$ copies/mouse in un-
160 pretreated mice **(Figure 3D)**. At 4 dpi, the lung viral loads were maintained in Ad5::hACE2-pretreated
161 mice (2.8 $\pm$ 1.3 $\times 10^9$ copies/mouse), whereas a drop to (1.7 $\pm$ 2.3) $\times 10^4$ or (3.9 $\pm$ 5.1) $\times 10^3$
162 copies/mouse was observed in empty Ad5-pretreated or unpretreated mice, respectively. At 7 dpi, in
163 Ad5::hACE2-pretreated mice, the viral loads decreased significantly, albeit were still largely detectable
164 ((1.33 $\pm$ 0.9) $\times 10^6$ copies/mouse).

165 Ad5::hACE-2 i.n. instillation induced $CD45^+$ cell recruitment to the lungs **(Figure 3E)**. However,
166 this effect was reduced with decreasing vector doses, as determined at day 4 post instillation. The dose

167 of 4×10^8 IGU/mouse did not cause $CD45^+$ cell recruitment, as compared to the PBS-treated controls,
168 but still conferred full permissibility to SARS-CoV-2 replication **(Figure 3F)**. The permissibility of
169 Ad5-hACE2-pretreated mice to SARS-CoV-2 replication and the set-up of this model paved the way
170 for the in vivo assessment of vaccine or drug efficacy against SARS-CoV-2 in mice.

171 **Evaluation of the protective potential of LV::S_{FL} against SARS-CoV-2 in mice**

172 To investigate the prophylactic potential of LV::S_{FL} against SARS-CoV-2, C57BL/6 mice (*n* =
173 4/group) were injected i.p. with a single dose of 1×10^7 TU/mouse of LV::S_{FL} or a negative control
174 LV (sham). At week 7 post immunization, mice were pretreated with Ad5::hACE2, and 4 days later,
175 inoculated i.n. with 1×10^5 $TCID_{50}$ of SARS-CoV-2 **(Figure 4A)**. At 3 dpi, the lung viral loads in
176 LV::S_{FL}-vaccinated mice was reduced by ~1 $\log_{10}$, i.e., Mean ± SEM of $(3.2 \pm 2.2) \times 10^8$ SARS-CoV-
177 2 RNA copies/mouse compared to $(1.7 \pm 0.9) \times 10^9$ or $(2.4 \pm 1.6) \times 10^9$ copies/mouse in the un- or
178 sham-vaccinated mice, respectively **(Figure 4B)**. Therefore, a single LV::S_{FL} injection effectively
179 afforded ~90% inhibition of the viral replication in the lungs.

180 To further improve the prophylactic effect, we evaluated the prime-boost or prime-target
181 approaches. C57BL/6 mice (*n* = 4-5/group) were primed i.p. with 1×10^7 TU/mouse of LV::S_{FL} or a
182 control LV at week 0, and then boosted at week 3 with: (i) 1×10^7 TU/mouse of the same LV via i.p.
183 ("LV::S_{FL} i.p-i.p.", prime-boost), or (ii) with 3×10^7 TU/mouse via i.n. ("LV::S_{FL} i.p.-i.n.", prime-
184 target) to attract the mediators of systemic immunity to the lung mucosa **(Figure 4C)**. The sera were
185 investigated after boost/target. Systemic boosting with LV::S_{FL} via i.p. resulted in a significant increase
186 in the anti-S_{CoV-2} IgG titers, which was more obvious when the binding was evaluated against the full
187 length S **(Figure 4D, left)**, compared to S1 or RBD fragment alone **(Supplemental Figure 2)**. This
188 observation may suggest that the concerned B-cell epitopes could be of conformational type. In
189 contrast, mucosal targeting with LV::S_{FL} via i.n. did not lead to a statistically significant improvement
190 of anti-S_{CoV-2} IgG titers at the systemic level **(Figure 4D left, Supplemental Figure 2)**. In terms of
191 serum neutralization potential, even though a trend to increase was observed after i.p. or i.n. boost, the
192 differences did not reach statistical significance **(Figure 4D right)**.

193 All the mice were then pretreated with Ad5::hACE2 and challenged with 0.3×10^5 $TCID_{50}$ of SARS-
194 CoV-2 at week 4. At 3 dpi, the lung viral loads were significantly lower in LV::S_{FL} i.p.-i.p. immunized
195 mice than in sham-vaccinated mice, i.e., $(6.8 \pm 3.7) \times 10^8$ vs $(1.1 \pm 1.6) \times 10^8$ copies of SARS-CoV-2
196 RNA/mouse, respectively **(Figure 4F)**. This viral load reduction was similar to that obtained with a
197 single LV::S_{FL} administration **(Figure 4B)**. However, most importantly, after i.n. LV::S_{FL} target
198 immunization, a sharp decrease of up to 4 $\log_{10}$ was observed in the viral loads compared to the sham-
199 vaccinated group, and 2 out of 5 mice achieved undetectable viral RNA in the lungs. Therefore,
200 increasing the nAb titers at the systemic levels does not necessarily improve the SARS-CoV-2-specific

201 protection, but a mucosal i.n. target immunization, which attracts the immune effectors to the site of
202 the potential viral infection, contributes substantially to the inhibition of SARS-CoV-2 replication.

203 Based on the compelling evidence of innate immune hyperactivity in the acute lung injury in
204 COVID-19 (Vabret et al., 2020), we investigated the possible variations of the lung innate immune cell
205 subsets **(Figure 5A)**, in the non-infected controls, sham-vaccinated or LV::S_{FL}-vaccinated mice
206 inoculated with SARS-CoV-2. At 3 dpi, we detected no differences in the proportions of basophils or
207 NK cells versus total lung $CD45^+$ cells among the experimental groups **(Figure 5B)**. In net contrast,
208 we detected increased proportions of alveolar macrophages, dendritic cells, mast cells, eosinophils,
209 $Ly6C^+$ or $Ly6C^-$ monocytes/macrophages or neutrophils versus total lung $CD45^+$ cells, in sham-
210 vaccinated mice which displayed the highest lung viral loads. These observations demonstrate that in
211 this mouse model, the increased lung SARS-CoV-2 loads are correlated with the recruitment of several
212 inflammation-related innate immune cells, and that vaccine-mediated anti-viral protection dampens or
213 avoids such inflammation. This was corroborated with the reduced cytokine and chemokine contents
214 in the lungs of mice vaccinated by prime-boost/target with LV::S_{FL}, as evaluated by qRT-PCR applied
215 to RNA extracted from the total lung homogenates **(Figure 5C)**. Therefore, the conferred protection
216 also avoided pulmonary inflammation linked to SARS-CoV-2 infection.

217 **Evaluation of the protective potential of LV::S_{FL} against SARS-CoV-2 in golden hamsters**

218 Outbred *Mesocricetus auratus*, so-called golden hamsters, provide a suitable pre-clinical model to
219 study the COVID-19 pathology, since the ACE2 ortholog of this species interacts efficaciously with
220 S_{CoV-2}, whereby host cell invasion and viral replication (Sia et al., 2020). We thus investigated the
221 prophylactic effect of LV::S_{FL} vaccination on SARS-CoV-2 infection in this pertinent model. Although
222 integrative LV are largely safe and passed successfully a phase 1 clinical trial (2011-006260-52 EN),
223 in addition to the LV::S_{FL}, we also evaluated an integrase deficient, non-integrative version of LV::$_{SFL}$
224 (NILV) with the prospect of application in future clinical trials.

225 To assess the prophylactic effect of vaccination following prime-boost/target regimen, *M. auratus*
226 hamsters (n = 6/group) were: (i) primed i.p. with a low dose of 1×10^6 TU of LV::S_{FL} and boosted i.n.
227 at week 5 with 4×10^7 TU of LV::S_{FL}, ("LV::S_{FL} i.p.-i.n. Low"), (ii) primed i.p. with a high dose of 1
228 $\times 10^7$ TU of LV::S_{FL} and boosted i.n. at week 5 with 4×10^7 TU of LV::S_{FL} ("LV::S_{FL} i.p.-i.n. High"),
229 or (iii) primed intramuscularly (i.m.) with 1×10^8 TU of NILV::S_{FL} and boosted i.n. at week 5 with the
230 same dose of NILV::S_{FL} ("NILV::S_{FL} i.m.-i.n.") **(Figure 6A)**. Sham-vaccinated controls received the
231 same amounts of an empty LV via i.p. and then i.n. routes. Strong and comparable S_{CoV-2}-specific IgG
232 antibodies were detected by ELISA in the sera of hamsters from the three vaccinated groups, before
233 and after the i.n. boost **(Figure 6B)**. Post boost/target serology detected neutralization activity in all
234 the groups, with the highest EC50 average observed in "int LV::S_{FL} i.p.-i.n. High" individuals. Such
235 levels were comparable to those detected in asymptomatic, pauci-symptomatic, symptomatic or healthy

236 COVID-19 contacts in humans **(Figure 6C)**. All the hamsters were challenged i.n. with 0.3×10^5
237 $TCID_{50}$ of SARS-CoV-2 at week 5. Up to 16% weight loss was progressively reached at 4 dpi in sham-
238 vaccinated individuals, compared to non-significant loss in all the LV::S_{FL}-vaccinated groups **(Figure**
239 **6D)**.

240 At 2 dpi, decreases of ~1.5-to-3 log_{10} were observed in the lung viral loads of "int LV::S_{FL} i.p.-i.n.
241 Low", "int LV::S_{FL} i.p.-i.n. High" and "non int LV::S_{FL} i.m.-i.n." groups, compared to sham-vaccinated
242 hamsters **(Figure 7A)**. At 4 dpi, the magnitude of viral load reductions in the vaccinated groups were
243 much more important and reached >4 log_{10}, compared to the sham-vaccinated individuals. As evaluated
244 by qRT-PCR in the total lung homogenates of the protected "int LV::S_{FL} i.p.-i.n. Low", "int LV::S_{FL}
245 i.p.-i.n. High" and "NILV::S_{FL} i.m.-i.n." groups, substantial decreases were observed in the expression
246 of inflammatory cytokines, for instance IFNγ and IL-6 — and the anti-inflammatory IL-10, the most
247 probably as a consequence of important inflammation — and CCL2, CCL3 and CXCL10 chemokines,
248 compared to their unprotected sham-vaccinated counterparts **(Figure 7B)**.

249 Altogether, based on a complete set of virological and immunological data, the LV::S_{FL} vector elicits
250 S_{CoV-2}-specific nAbs and T-cell responses, correlative with substantial level of protection against
251 SARS-CoV-2 infection in two pertinent animal models, and notably upon mucosal i.n. administration.

252

253 **Discussion**

254 Prophylactic strategies are necessary to control SARS-CoV-2 infection which, 6 months into the
255 pandemic, still continues to spread exponentially without sign of slowing down. It is now demonstrated
256 that primary infection with SARS-CoV-2 in rhesus macaques leads to protective immunity against re-
257 exposure (Chandrashekar et al., 2020). Numerous vaccine candidates, based on naked DNA (Yu et al.,
258 2020) or mRNA, recombinant protein, replicating or non-replicating viral vectors, including adenoviral
259 Ad5 vector (Zhu et al., 2020), or alum-adjuvanted inactivated virus (Gao et al., 2020) are under active
260 development for COVID-19 prevention. Our immunologic rationale for selecting LV to deliver gene
261 encoding S_{CoV-2} antigen is based on the insights obtained on the efficacy of heterologous gene
262 expression *in situ*, as well as the longevity and composite nature of humoral and cell-mediated
263 immunity elicited by this immunization platform. Unique to LV is the ability to transduce proliferating
264 and non-dividing cells such as dendritic cells (Esslinger et al., 2002; Firat et al., 2002; He et al., 2005),
265 thereby LV serves as a powerful vaccination strategy (Beignon et al., 2009; Buffa et al., 2006; Coutant
266 et al., 2012; Gallinaro et al., 2018; Iglesias et al., 2006) to provoke strong and long-lasting adaptive
267 responses (Cousin et al., 2019; Ku et al., Submitted.). Notably, in sharp contrast to many other viral
268 vectors, LV do not suffer from pre-existing immunity in populations, which is linked to their pseudo-
269 typing with the glycoprotein envelope from Vesicular Stomatitis Virus, to which humans are barely
270 exposed. We recently demonstrated that a single injection of a LV expressing Zika envelope provides
271 a rapid and durable protection against Zika infection (Ku et al., 2020). Our recent comprehensive
272 systematic comparison of LV to the gold standard Ad5 immunization vector also documented the
273 superiority of LV to induce multifunctional and central memory T cells in the mouse model, and
274 stronger immunogenicity in outbred rats (Ku et al., Submitted.), underlining the largely adapted
275 properties of LV for vaccinal applications.

276 Linked to the absence of permissibility of laboratory mice to SARS-CoV-2 replication and the
277 current unavailability of hACE2 transgenic mice in Europe, we set up an *in vivo* transduction murine
278 model in which the hACE2 expression is induced in the respiratory tracts by an i.n. Ad5::hACE2
279 pretreatment prior to SARS-CoV-2 inoculation. This approach renders mice largely permissive to
280 SARS-CoV-2 replication in the lungs and allows assessment of vaccine or drug efficacy against this
281 virus. This method has also been successfully used to establish the expression of human DPP4 for the
282 study of mouse infection with MERS-CoV (Zhao et al., 2014). Even though the Ad5::hACE2 model
283 may not fully mimic the physiological ACE2 expression profile and thus may not reflect all the aspects
284 of the pathophysiology of SARS-CoV-2 infection, it provides a pertinent model to evaluate *in vivo* the
285 effects of anti-viral drugs, vaccine candidates, various mutations or genetic backgrounds on the SARS-
286 CoV-2 replication. By using a low dose of Ad5::hACE2/mouse, no particular $CD45^+$ cell recruitments

287 were detectable at day 4 post instillation, indicative of an absence of Ad5-related inflammation before
288 the inoculation of SARS-CoV-2.

289 We first evaluated the efficacy of LV each encoding one of the variants of S, i.e., full-length,
290 membrane anchored (LV::S_{FL}), S1-S2 ecto-domain, devoid of the transmembrane and C-terminal short
291 internal tail (LV::S1-S2), or S1 alone (LV::S1). Even though a single administration of each of these
292 LV was able to induce high anti-S_{CoV-2} Ab titers, only LV::S_{FL} was able to induce highly functional
293 nAbs. Such single-injection of LV-based vaccine induced a neutralizing activity, which on average
294 was comparable to those found in a cohort of SARS-CoV-2 patients exhibiting mild symptoms. This
295 finding predicted a protective potential of the humoral responses induced by the LV::S_{FL} vector. In
296 parallel, S-specific $CD4^+$ and $CD8^+$ T-cell responses were also observed in the spleen of mice as early
297 as 2 weeks after a single LV::S_{FL} injection, as detected against a single MHC-II- and numerous MHC-
298 I-restricted immunogenic regions that we identified in C57BL/6 (H-2^b) mice.

299 In the transduced mouse model which allows high rate of SARS-CoV-2 replication, vaccination by
300 a single i.p. administration of 1 x 10^7 TU of LV::S_{FL}, 6 weeks before the virus inoculation, was
301 sufficient to inhibit the viral replication by ~1 $\log_{10}$. Further boosting via the systemic route did not
302 afford improved protection rate when compared to a single administration. However, priming by
303 systemic route and boosting via mucosal route inhibited efficiently viral replication and avoided lung
304 inflammation. Such protection was correlated with high titers of anti-S_{CoV-2} IgG and a strong
305 neutralization activity in sera. Additional experiments in appropriate KO mice or adoptive immune cell
306 transfer approaches will be necessary to identify the immunological pathways that contribute to disease
307 severity or protection against SARS-CoV-2. Both nAbs and cell-mediated immunity, both very
308 efficaciously induced with the LV-based vaccine candidate, may synergize to blockade infection and
309 viral replication.

310 Ab-Dependent Enhancement (ADE) of coronavirus entry to the host cells has been evoked as a
311 potential obstacle in vaccination against coronaviruses. With DNA (Yu et al., 2020) or inactivated
312 SARS-CoV-2 virus (Gao et al., 2020) vaccination in macaques, no immunopathological exacerbation
313 has been observed but could not be excluded. Long term observation even after decrease in Ab titer
314 could be necessary to exclude such hypothesis. In the case of MERS-CoV, it has been reported that
315 one particular RBD-specific neutralizing monoclonal Ab (Mersmab1), by mimicking the viral receptor
316 human DPP4 and inducing conformational rearrangements of S_{MERS}, can mediate in vitro ADE of
317 MERS-CoV into the host cells (Wan et al., 2020). We believe that it is difficult to compare the
318 polyclonal Ab response and its paratope repertoire complexity with the singular properties of a
319 monoclonal Ab which cannot be representative of the polyclonal response induced by a vaccine. In
320 addition, very contradictorily, results from the same team reported that a single-dose treatment with a
321 humanized version of Mersmab1 afforded complete protection of a human transgenic mouse model

322 from lethal MERS challenge (Qiu et al., 2016). Therefore, even with an Ab which could facilitate the
323 cell host invasion in vitro in some conditions, not only there is no exacerbation of the infection in vivo,
324 but also there is a notable protection.

325 Substantial degrees of protection against SARS-CoV-2 infection and reduction in the lung
326 inflammation were observed also in *M. auratus* golden hamsters immunized following prime-
327 boost/target regimen with either integrative LV or NILV::S_{FL}. Confirmation of the protection results
328 in this highly sensitive species further favors the LV::S_{FL} vaccine candidate, especially under its non-
329 integrative form, for future introduction into clinical trials.

330 Prophylactic vaccination is the most cost-effective and efficient strategy against infectious diseases
331 in general and against emerging coronaviruses in particular. Our results provide strong evidence that
332 the LV coding for S_{FL} protein of SARS-CoV-2, used via the mucosal route of vaccination, represents
333 a promising vaccine candidate against COVID-19.

334

335

336 **Material and Methods**

337 **Construction of transfer pFLAP plasmids coding for S_{FL}, S1-S2, or S1 proteins**

338 A codon-optimized full-length S (1-1273) sequence was amplified from pMK-RQ_S-2019-nCoV
339 and inserted between BamHI and XhoI sites of pFlap-ieCMV-WPREm. Sequences encoding for S1-
340 S2 (1-1211) or S1 (1-681) were amplified by PCR from the pFlap-ieCMV- S_{FL}-WPREm plasmid and
341 sub-cloned into pFlap-ieCMV-WPREm between the BamHI and XhoI restriction sites **(Supplemental**
342 **Figure 1)**. Each of the PCR products were inserted between the native human ieCMV promoter and a
343 mutated Woodchuck Posttranscriptional Regulatory Element (mWPRE) sequence, where a mutation
344 was introduced to avoid expression of the X protein. Plasmids were amplified in *Escherichia coli* DH5a
345 in Lysogeny Broth supplemented with 50 µg/ml of kanamycin and purified using the NucleoBond Xtra
346 Maxi EF Kit (Macherey Nagel) and resuspended in Tris-EDTA Endotoxin-Free buffer overnight.
347 Plasmid were quantified with a NanoDrop 2000c spectrophotometer (Thermo Scientific), aliquoted
348 and stored at -20°C. Plasmid DNA were verified by enzymatic digestion and by sequencing the region
349 proximal to the transgene insertion sites.

350 **Production and titration of LV**

351 Non-replicative LV were produced in Human Embryonic Kidney (HEK)-293T cells, as previously
352 detailed (Zennou et al., 2000). Briefly, lentiviral particles were produced by transient calcium
353 phosphate co-transfection of HEK293T cells with the vector plasmid pTRIP/sE, a VSV-G Indiana
354 envelope plasmid and an encapsidation plasmid (p8.74 or pD64V for the production of integration-
355 proficient or integration-deficient vectors respectively). Supernatants were harvested at 48h post
356 transfection, clarified by 6-minute centrifugation at 2500 rpm at 4°C. LV were aliquoted and stored at
357 -80°C. Vector titers were determined by transducing 293T cells treated with aphidicolin. The titer,
358 proportional to the efficacy of nuclear gene transfer, is determined as Transduction Unit (TU)/ml by
359 qPCR on total lysates at day 3 post transduction, by use of forward 5'-TGG AGG AGG AGA TAT
360 GAG GG-3' and reverse 5'-CTG CTG CAC TAT ACC AGA CA-3' primers, specific to pFLAP
361 plasmid and forward 5'-TCT CCT CTG ACT TCA ACA GC-3' and reverse 5'-CCC TGC ACT TTT
362 TAA GAG CC-3' primers specific to the host housekeeping gene *gadph* as previously described
363 (Iglesias et al., 2006).

364 **Mouse and hamster studies**

365 Female C57BL/6JRj mice (Janvier, Le Genest Saint Isle, France) were used between the age of 6
366 and 10 weeks. Male *Mesocricetus auratus* golden hamsters (Janvier, Le Genest Saint Isle, France) were
367 purchased mature, i.e. 80-90 gr weight. At the beginning of the immunization regimen they weigh
368 between 100 and 120 gr. Experimentation on animals was performed in accordance with the European
369 and French guidelines (Directive 86/609/CEE and Decree 87-848 of 19 October 1987) subsequent to

370 approval by the Institut Pasteur Safety, Animal Care and Use Committee, protocol agreement delivered
371 by local ethical committee (CETEA #DAP20007) and Ministry of High Education and Research
372 APAFIS#24627-2020031117362508 v1. Animals were vaccinated with the indicated TU of LV and
373 sera were collected at various time points post immunization to monitor binding and neutralization
374 activities. Previous to i.m. or i.n. instillations, animals were anesthetized by i.p. injection of a mixture
375 of Ketamine (Imalgene, 50 mg/kg) and Xylazine (Rompun, 50 mg/kg).

376 **SARS-CoV-2 inoculation**

377 Ad5::hACE2-pretreated hamsters or mice were anesthetized by i.p. injection of mixture Ketamine
378 and Xylazine, transferred into a biosafety cabinet 3 where they were inoculated respectively with 0.3
379 and 1×10^5 $TCID_{50}$ of a SARS-CoV-2 clinical isolate amplified in VeroE6 cells, provided by the Centre
380 National de Réference des Virus Respiratoires, France. The viral inoculum was contained in 20 µl for
381 mice and in 50 µl for hamsters. Animals were then housed in an isolator in BSL3 animal facilities of
382 Institut Pasteur. The organs and fluids recovered from the infected animals, with live SARS-CoV-2
383 were manipulated following the approved standard operating procedures of the BioSafety Level BSL3
384 facilities.

385 **Recombinant S_{CoV-2} proteins**

386 Codon-optimized nucleotide fragments encoding a stabilized foldon-trimerized version of the
387 SARS-CoV-2 S ectodomain (a.a. 1 to 1208), the S1 monomer (a.a. 16 to 681) and the RBD subdomain
388 (amino acid 331 to 519) both preceded by a murine IgK leader peptide and followed by an 8xHis Tag
389 were synthetized and cloned into pcDNA™3.1/Zeo$^{(+)}$ expression vector (Thermo Fisher Scientific).
390 Proteins were produced by transient co-transfection of exponentially growing Freestyle™ 293-F
391 suspension cells (Thermo Fisher Scientific, Waltham, MA) using polyethylenimine (PEI)-precipitation
392 method as previously described (Lorin and Mouquet, 2015). Recombinant S_{CoV-2} proteins were purified
393 by affinity chromatography using the Ni Sepharose® Excel Resin according to manufacturer's
394 instructions (Thermo Fisher Scientific). Protein purity was evaluated by in-gel protein silver-staining
395 using Pierce Silver Stain kit (Thermo Fisher Scientific) following SDS-PAGE in reducing and non-
396 reducing conditions using NuPAGE™ 3-8% Tris-Acetate gels (Life Technologies). Purified proteins
397 were dialyzed overnight against PBS using Slide-A-Lyzer® dialysis cassettes (10 kDa MW cut-off,
398 Thermo Fisher Scientific). Protein concentration was determined using the NanoDrop™ One
399 instrument (Thermo Fisher Scientific).

400 **ELISA**

401 Ninety-six-well Nunc Polysorp plates (Nunc, Thermo Scientific) were coated overnight at 4 °C with
402 100 ng/well of purified S_{CoV-2} proteins in carbonate buffer pH 9.6. The next day, plates were blocked

403 with carbonate buffer containing 1% BSA for 2 h at 37°C. Wells were then washed with PBS
404 containing 0.05% Tween 20 (PBS-T), 1:100-diluted sera in PBS-T containing 1% BSA and four serial
405 ten-to-ten dilutions were added and incubated during 2h at 37°C. After PBS-T washings, plates were
406 incubated with 1,000-fold diluted peroxydase-conjugated goat anti-mouse IgG (Jackson
407 ImmunoResearch Europe Ltd, Cambridgeshire, United Kingdom) for 1 h. Plates were revealed by
408 adding 100 µl of 3,3',5,5'-tetramethylbenzidine chromogenic substrate (Eurobio Scientific). Following
409 a 30 min incubation, reaction was stopped by adding 100 µl of 2N H2SO4 and optical densities were
410 measured at 450nm/620nm on a PR3100 reader.

411 **nAb Detection**

412 Serial dilutions of heat inactivated sera were assessed for nAbs via an inhibition assay which uses
413 HEK293T cells transduced to stably express human ACE2 and non-replicative S_{CoV-2} pseudo-typed LV
414 particles which harbor the reporter *luciferase firefly* gene, allowing quantitation of the host cell
415 invasion by mimicking fusion step of native SARS-CoV-2 virus (Sterlin et al.). First, 1.5×10^2 TU of
416 S_{CoV-2} pseudo-typed LV were pre-incubated, during 30 min at room temperature, in U-bottom plates,
417 with serial dilutions of each serum in a final volume of 50µl in DMEM-glutamax, completed with 10%
418 heat-inactivated FCS and 100 U/ml penicillin and 100 µg/ml streptomycin. The samples were then
419 transferred into clear-flat-bottom 96-well-black-plates, and each well received 2×10^4 $hACE2^+$
420 HEK293-T cells, counted in a NucleoCounter NC.200 system (Chemometec, Denmark) contained in
421 50 µl. After 2 days incubation at 37°C 5% CO_2, the transduction efficiency of $hACE2^+$ HEK293-T
422 cells by pseudo-typed LV particles was determined by measuring the luciferase activity, using a
423 Luciferase Assay System (Promega) on an EnSpire plate reader (PerkinElmer). Results are expressed
424 as percentages of inhibition of luciferase activity compared to the maximum of luciferase activity in
425 the absence of nAbs.

426 **S_{FL} T-cell epitope mapping**

427 In order to map the immuno-dominant epitopes of S_{CoV-2}, peptides spanning the whole S_{FL}
428 (Mimotopes, Australia) were pooled by 25, each containing 15 a.a. residues overlapping by 10 a.a.
429 Peptides were dissolved in DMSO at a concentration of 2 mg/ml and diluted before use at 1 µg/ml (for
430 ELISPOT) or 2–5 µg/mL (for ICS) in α-MEM medium supplemented with 10% FCS, 100 U/ml
431 penicillin and 100 µg/ml streptomycin, 1 x 10-4 M non-essential amino-acids, 1% vol/vol HEPES, 1 x
432 10-3 M sodium pyruvate and 5×10^{-5} M of β-mercapto-ethanol before use in functional assays. IFN-γ
433 ELISPOT and ICS assays were performed as described previously (Bourgine et al., 2018). For ICS,
434 cells were acquired in an Attune NxT Flow cytometer (ThermoFisher Scientific) and the data were
435 analyzed by FlowJo Software (TreeStar Inc.).

436 **Generation of Ad5 gene transfer vectors and intranasal pretreatment of mice**

437 The Ad5 gene transfer vectors were produced by the use of ViraPower Adenoviral Promoterless
438 Gateway Expression Kit (Thermo Fisher Scientific, France). The sequence containing CMV promoter,
439 BamH1/Xho1 restriction sites and WPRE was PCR amplified from the pTRIPΔU3CMV plasmid, by
440 use of: (i) forward primer, encoding the attB1 in the 5' end, and (ii) reverse primer, encoding both the
441 attB2 and SV40 polyA signal sequence in the 5' end. The attB-PCR product was cloned into the
442 gateway pDORN207 donor vector, via BP Clonase reaction. The *hACE2* was amplified from a plasmid
443 derivative of hACE2-expressing pcDNA3.1[1] (generous gift from Nicolas Escriou) while e*gfp* was
444 amplified from pTRIP-ieCMV-eGFP-WPRE[2]. The amplified PCR products were cloned into the
445 pDORN207 plasmid via the BamH1 and Xho1 restriction sites. To obtain the final Ad5 plasmid, the
446 pDORN207 vector, harboring *hACE2* or *gfp* genes, was further inserted into pAd/PL-DEST™ vector
447 via LR Clonase reaction **(Supplementary Figure 3).**

448 The Ad5 virions were generated by transfecting the E3-transcomplementing HEK-293A cell line
449 with pAd CMV-GFP-WPRE-SV40 polyA or pAd CMV-hACE2-WPRE-SV40 polyA plasmid
450 followed by subsequent vector amplification, according to the manufacturer's protocol (ViraPower
451 Adenoviral Promoterless Gateway Expression Kit, Thermo Fisher Scientific). The Ad5 particles were
452 purified using Adeno-X rapid Maxi purification kit and concentrated with the Amicon Ultra-4 10k
453 centrifugal filter unit. Vectors were resuspended and stocked à -80°C in PIPES buffer pH 7.5,
454 supplemented with 2.5% glucose. Ad5 were titrated using qRT-PCR protocol, as described by Gallaher
455 et al (Gallaher and Berk, 2013), adapted to HEK-293T cells.

456 **Western blot**

457 Expression of hACE2 in the lungs of Ad5::hACE2-transduced mice was assessed by Western
458 Blotting. One × 10^6 cells from lung homogenate were resolved on 4 – 12 % NuPAGE Bis-Tris protein
459 gels (Thermo Fisher Scientific, France), then transferred onto a nitrocellulose membrane (Biorad,
460 France). The nitrocellulose membrane was blocked in 5 % non-fat milk in PBS-T for 2 hours at room
461 temperature and probed overnight with goat anti-hACE2 primary Ab at 1 µg/mL (AF933, R&D
462 systems). Following three washing intervals of 10 minutes with PBS-T, the membrane was incubated
463 for 1 hour at room temperature with HRP-conjugated anti-goat secondary Ab and HRP-conjugated
464 anti-β-actin (ab197277, Abcam). The membrane was washed with PBS-T thrice before visualization
465 with enhanced chemiluminescence via the super signal west femto maximum sensitivity substrate
466 (ThermoFisher, France) on ChemiDoc XRS+ (Biorad, France). PageRuler Plus prestained protein
467 ladder was used as size reference.

468 **Determination of SARS-CoV-2 viral loads in the lungs**

469 Half of each lung lobes were removed aseptically and frozen at -80°C. Organs were thawed and
470 homogenized for 20 s at 4.0 m/s, using lysing matrix M (MP Biomedical) in 500 µl of ice-cold PBS.

471 The homogenization was performed in an MP Biomedical Fastprep 24 Tissue Homogenizer. The
472 homogenates were centrifuged 10 min at 2000g for further RNA extraction from the supernatants.
473 Particulate viral RNA was extracted from 70 µl of such supernatants using QIAamp Viral RNA Mini
474 Kit (Qiagen) according to the manufacturer's procedure. Viral load was determined following reverse
475 transcription and real-time TaqMan® PCR essentially as described (Corman et al., 2020), using
476 SuperScriptTM III Platinum One-Step Quantitative RT-PCR System (Invitrogen) and primers and
477 probe (Eurofins) targeting S_{CoV-2} gene as listed in **(Supplemental Table 1)**. In vitro transcribed RNA
478 derived from plasmid pCI/SARS-CoV envelope was synthesized using T7 RiboMAX Express Large
479 Scale RNA production system (Promega), then purified by phenol/chloroform extractions and two
480 successive precipitations with ethanol. RNA concentration was determined by optical density
481 measurement, then RNA was diluted to 10^9 genome equivalents/µL in RNAse-free water containing
482 100µg/mL tRNA carrier, and stored in single-use aliquots at -80°C. Serial dilutions of this in vitro
483 transcribed RNA were prepared in RNAse-free water containing 10µg/ml tRNA carrier and used to
484 establish a standard curve in each assay. Thermal cycling conditions were: (i) reverse transcription at
485 55°C for 10 min, (ii) enzyme inactivation at 95°C for 3 min, and (iii) 45 cycles of
486 denaturation/amplification at 95°C for 15 s, 58°C for 30 s. Products were analyzed on an ABI 7500
487 Fast real-time PCR system (Applied Biosystems).

488 **Cytometric analysis of lung innate immune cells**

489 Lungs from individual mice were treated with collagenase-DNAse-I for a 30-minute incubation at
490 37°C and homogenized by use of GentleMacs. Cells were filtered through 100 µm-pore filters and
491 centrifuged at 1200 rpm during 8 minutes. Cells were then treated with Red Blood Cell Lysing Buffer
492 (Sigma) and washed twice in PBS. Cells were stained as following. (i) To detect DC, monocytes,
493 alveolar and interstitial macrophages: Near IR Live/Dead (Invitrogen), FcγII/III receptor blocking anti-
494 CD16/CD32 (BD Biosciences), BV605-anti-CD45 (BD Biosciences), PE-anti-CD11b (eBioscience),
495 PE-Cy7-antiCD11c (eBioscience), BV450-anti-CD64 (BD Biosciences), FITC-anti-CD24 (BD
496 Biosciences), BV711-anti-CD103 (BioLegend), AF700-anti-MHC-II (BioLegend), PerCP-Cy5.5-anti-
497 Ly6C (eBioscience) and APC anti-Ly-6G (Miltenyi) mAbs, (ii) to detect neutrophils or eosinophils:
498 Near IR DL (Invitrogen), FcγII/III receptor blocking anti-CD16/CD32 (BD Biosciences), PerCP-
499 Vio700-anti-CD45 (Miltenyi), APC-anti-CD11b (BD Biosciences), PE-Cy7-anti-CD11c
500 (eBioscience), FITC-anti-CD24 (BD Biosciences), AF700-anti-MHC-II (BioLegend), PE-anti-Ly6G
501 (BioLegend), BV421-anti-Siglec-F (BD Biosciences), (iii) to detect mast cells, basophils, NK: Near
502 IR DL (Invitrogen), BV605-anti-CD45 (BD Biosciences), PE-anti-CD11b (eBioscience), eF450-anti-
503 CD11c (eBioscience), PE-Cy7-anti-CD117 (BD Biosciences), APC-anti-FcER1 (BioLegend), AF700-
504 anti-NKp46 (BD Biosciences), FITC-anti-CCR3 (BioLegend), without FcγII/III receptor blocking
505 anti-CD16/CD32. Cells were incubated with appropriate mixtures for 25 minutes at 4°C, washed twice

506 in PBS containing 3% FCS and then fixed with Paraformaldehyde 4% by an overnight incubation at
507 4°C. The cells were acquired in on Attune NxT cytometer system (Invitrogen) and data were analyzed
508 by FlowJo software (Treestar, OR, USA).

509 **qRT-PCR Detection of inflammatory cytokines and chemokines in the lungs of the mice and**
510 **hamsters**

511 Lung samples from mice or hamsters were added to lysing matrix D (MP Biomedical) containing 1
512 mL of TRIzol reagent and homogenized at 30 s at 6.0 m/s twice using MP Biomedical Fastprep 24
513 Tissue Homogenizer. Total RNA was extracted using TRIzol reagent (ThermoFisher Scientific,
514 France) according to the manufacturer's procedure. cDNA was synthesized from 4 µg of RNA in the
515 presence of 2.5 µM of oligo(dT) 18 primers, 0.5 mM of deoxyribonucleotides, 2.0 U of RNase Inhibitor
516 and SuperScript IV Reverse Transcriptase (ThermoFisher Scientific, France) in 20 µl reaction. The
517 real-time PCR was performed on QuantStudio™ 7 Flex Real-Time PCR System (ThermoFisher
518 Scientific, France). Reactions were performed in triplicates in a final reaction volume of 10 µl
519 containing 5 µl of iQ™ SYBR® Green Supermix (Biorad, France), 4 µl of cDNA diluted 1:15 in
520 DEPC-water and 0.5 µl of each forward and reverse primers at a final concentration of 0.5 µM
521 **(Supplementary Table 2 and 3)**. The following thermal profile was used: a single cycle of polymerase
522 activation for 3 min at 95°C, followed by 40 amplification cycles of 15 sec at 95°C and 30 sec 60°C
523 (annealing-extension step). Mice β-globin or hamster ribosomal protein L18 (RLP18) was used as an
524 endogenous reference control to normalize differences in the amount of input nucleic acid. The average
525 C_T values were calculated from the technical replicates for relative quantification of target
526 cytokines/chemokines. The differences in the C_T cytokines/chemokines amplicons and the C_T of the
527 endogenous reference control, termed ΔC_T, were calculated to normalize for differences in the quantity
528 of nucleic acid. The ΔC_T of the experimental condition compared relatively to the PBS-immunized
529 individuals using the comparative $\Delta\Delta C_T$ method. The fold change in gene expression was further
530 calculated using $2^{-\Delta\Delta C_T}$.

531

532 **References**

533 Amanat, F., and F. Krammer. 2020. SARS-CoV-2 Vaccines: Status Report. *Immunity* 52:583-589.

534 Beignon, A.S., K. Mollier, C. Liard, F. Coutant, S. Munier, J. Riviere, P. Souque, and P. Charneau.
535 2009. Lentiviral vector-based prime/boost vaccination against AIDS: pilot study shows
536 protection against Simian immunodeficiency virus SIVmac251 challenge in macaques. *J Virol*
537 83:10963-10974.

538 Belouzard, S., V.C. Chu, and G.R. Whittaker. 2009. Activation of the SARS coronavirus spike protein
539 via sequential proteolytic cleavage at two distinct sites. *Proc Natl Acad Sci U S A* 106:5871-
540 5876.

541 Bourgine, M., S. Crabe, Y. Lobaina, G. Guillen, J.C. Aguilar, and M.L. Michel. 2018. Nasal route
542 favors the induction of CD4(+) T cell responses in the liver of HBV-carrier mice immunized
543 with a recombinant hepatitis B surface- and core-based therapeutic vaccine. *Antiviral Res*
544 153:23-32.

545 Buffa, V., D.R. Negri, P. Leone, M. Borghi, R. Bona, Z. Michelini, D. Compagnoni, C. Sgadari, B.
546 Ensoli, and A. Cara. 2006. Evaluation of a self-inactivating lentiviral vector expressing simian
547 immunodeficiency virus gag for induction of specific immune responses in vitro and in vivo.
548 *Viral Immunol* 19:690-701.

549 Chandrashekar, A., J. Liu, A.J. Martinot, K. McMahan, N.B. Mercado, L. Peter, L.H. Tostanoski, J.
550 Yu, Z. Maliga, M. Nekorchuk, K. Busman-Sahay, M. Terry, L.M. Wrijil, S. Ducat, D.R.
551 Martinez, C. Atyeo, S. Fischinger, J.S. Burke, M.D. Slein, L. Pessaint, A. Van Ry, J.
552 Greenhouse, T. Taylor, K. Blade, A. Cook, B. Finneyfrock, R. Brown, E. Teow, J. Velasco, R.
553 Zahn, F. Wegmann, P. Abbink, E.A. Bondzie, G. Dagotto, M.S. Gebre, X. He, C. Jacob-Dolan,
554 N. Kordana, Z. Li, M.A. Lifton, S.H. Mahrokhian, L.F. Maxfield, R. Nityanandam, J.P.
555 Nkolola, A.G. Schmidt, A.D. Miller, R.S. Baric, G. Alter, P.K. Sorger, J.D. Estes, H. Andersen,
556 M.G. Lewis, and D.H. Barouch. 2020. SARS-CoV-2 infection protects against rechallenge in
557 rhesus macaques. *Science. May 2020:eabc4776. doi: 10.1126/science.abc4776. PMID:*
558 *32434946.*

559 Corman, V., T. Bleicker, S. Brünink, and C. Drosten. 2020. Diagnostic detection of 2019-nCoV by
560 real-time RT-PCR. https://www.who.int/docs/default-source/coronaviruse/protocol-v2-1.pdf

561 Cousin, C., M. Oberkampf, T. Felix, P. Rosenbaum, R. Weil, S. Fabrega, V. Morante, D. Negri, A.
562 Cara, G. Dadaglio, and C. Leclerc. 2019. Persistence of Integrase-Deficient Lentiviral Vectors
563 Correlates with the Induction of STING-Independent CD8(+) T Cell Responses. *Cell Rep*
564 26:1242-1257 e1247.

565 Coutant, F., R.Y. Sanchez David, T. Felix, A. Boulay, L. Caleechurn, P. Souque, C. Thouvenot, C.
566 Bourgouin, A.S. Beignon, and P. Charneau. 2012. A nonintegrative lentiviral vector-based
567 vaccine provides long-term sterile protection against malaria. *PLoS One* 7:e48644.

568 Coutard, B., C. Valle, X. de Lamballerie, B. Canard, N.G. Seidah, and E. Decroly. 2020. The spike
569 glycoprotein of the new coronavirus 2019-nCoV contains a furin-like cleavage site absent in
570 CoV of the same clade. *Antiviral Res* 176:104742.
571 Di Nunzio, F., T. Felix, N.J. Arhel, S. Nisole, P. Charneau, and A.S. Beignon. 2012. HIV-derived
572 vectors for therapy and vaccination against HIV. *Vaccine* 30:2499-2509.
573 Esslinger, C., P. Romero, and H.R. MacDonald. 2002. Efficient transduction of dendritic cells and
574 induction of a T-cell response by third-generation lentivectors. *Hum Gene Ther* 13:1091-1100.
575 Firat, H., V. Zennou, F. Garcia-Pons, F. Ginhoux, M. Cochet, O. Danos, F.A. Lemonnier, P. Langlade-
576 Demoyen, and P. Charneau. 2002. Use of a lentiviral flap vector for induction of CTL immunity
577 against melanoma. Perspectives for immunotherapy. *J Gene Med* 4:38-45.
578 Gallaher, S.D., and A.J. Berk. 2013. A rapid Q-PCR titration protocol for adenovirus and helper-
579 dependent adenovirus vectors that produces biologically relevant results. *J Virol Methods*
580 192:28-38.
581 Gallinaro, A., M. Borghi, R. Bona, F. Grasso, L. Calzoletti, L. Palladino, S. Cecchetti, M.F. Vescio,
582 D. Macchia, V. Morante, A. Canitano, N. Temperton, M.R. Castrucci, M. Salvatore, Z.
583 Michelini, A. Cara, and D. Negri. 2018. Integrase Defective Lentiviral Vector as a Vaccine
584 Platform for Delivering Influenza Antigens. *Front Immunol* 9:171.
585 Gao, Q., L. Bao, H. Mao, L. Wang, K. Xu, M. Yang, Y. Li, L. Zhu, N. Wang, Z. Lv, H. Gao, X. Ge,
586 B. Kan, Y. Hu, J. Liu, F. Cai, D. Jiang, Y. Yin, C. Qin, J. Li, X. Gong, X. Lou, W. Shi, D. Wu,
587 H. Zhang, L. Zhu, W. Deng, Y. Li, J. Lu, C. Li, X. Wang, W. Yin, Y. Zhang, and C. Qin. 2020.
588 Rapid development of an inactivated vaccine candidate for SARS-CoV-2. *Science. 2020 Jul*
589 *3;369(6499):77-81. doi: 10.1126/science.abc1932. Epub 2020 May 6.PMID: 32376603.*
590 Guo, Y.R., Q.D. Cao, Z.S. Hong, Y.Y. Tan, S.D. Chen, H.J. Jin, K.S. Tan, D.Y. Wang, and Y. Yan.
591 2020. The origin, transmission and clinical therapies on coronavirus disease 2019 (COVID-19)
592 outbreak - an update on the status. *Mil Med Res* 7:11.
593 He, Y., J. Zhang, Z. Mi, P. Robbins, and L.D. Falo, Jr. 2005. Immunization with lentiviral vector-
594 transduced dendritic cells induces strong and long-lasting T cell responses and therapeutic
595 immunity. *J Immunol* 174:3808-3817.
596 Hu, B., A. Tai, and P. Wang. 2011. Immunization delivered by lentiviral vectors for cancer and
597 infectious diseases. *Immunol Rev* 239:45-61.
598 Iglesias, M.C., M.P. Frenkiel, K. Mollier, P. Souque, P. Despres, and P. Charneau. 2006. A single
599 immunization with a minute dose of a lentiviral vector-based vaccine is highly effective at
600 eliciting protective humoral immunity against West Nile virus. *J Gene Med* 8:265-274.
601 Ku, M.W., F. Anna, F. Souque, S. Petres, M. Prot, E. Simon-Loriere, P. Charneau, and M. Bourgine.
602 2020. A Single Dose of NILV-Based Vaccine Provides Rapid and Durable Protection against

603 Zika Virus. *Mol Ther. 2020 May 20;S1525-0016(20)30250-1. doi:*
604 *10.1016/j.ymthe.2020.05.016.*
605 Ku, M.W., P. Authié, P. Souque, M. Bourgine, M. Romano, P. Charneau, and L. Majlessi. Submitted.
606 High-Quality Memory T Cells by Programmed Antigen Expression in Dendritic Cells
607 Induced by Lentiviral Vector.
608 Lai, A.L., J.K. Millet, S. Daniel, J.H. Freed, and G.R. Whittaker. 2017. The SARS-CoV Fusion Peptide
609 Forms an Extended Bipartite Fusion Platform that Perturbs Membrane Order in a Calcium-
610 Dependent Manner. *J Mol Biol* 429:3875-3892.
611 Lorin, V., and H. Mouquet. 2015. Efficient generation of human IgA monoclonal antibodies. *J*
612 *Immunol Methods* 422:102-110.
613 Qiu, H., S. Sun, H. Xiao, J. Feng, Y. Guo, W. Tai, Y. Wang, L. Du, G. Zhao, and Y. Zhou. 2016.
614 Single-dose treatment with a humanized neutralizing antibody affords full protection of a
615 human transgenic mouse model from lethal Middle East respiratory syndrome (MERS)-
616 coronavirus infection. *Antiviral Res* 132:141-148.
617 Rosenberg, S.A., Y. Zhai, J.C. Yang, D.J. Schwartzentruber, P. Hwu, F.M. Marincola, S.L. Topalian,
618 N.P. Restifo, C.A. Seipp, J.H. Einhorn, B. Roberts, and D.E. White. 1998. Immunizing patients
619 with metastatic melanoma using recombinant adenoviruses encoding MART-1 or gp100
620 melanoma antigens. *J Natl Cancer Inst* 90:1894-1900.
621 Schirmbeck, R., J. Reimann, S. Kochanek, and F. Kreppel. 2008. The immunogenicity of adenovirus
622 vectors limits the multispecificity of CD8 T-cell responses to vector-encoded transgenic
623 antigens. *Mol Ther* 16:1609-1616.
624 Sia, S.F., L.M. Yan, A.W.H. Chin, K. Fung, K.T. Choy, A.Y.L. Wong, P. Kaewpreedee, R. Perera,
625 L.L.M. Poon, J.M. Nicholls, M. Peiris, and H.L. Yen. 2020. Pathogenesis and transmission of
626 SARS-CoV-2 in golden hamsters. *Nature. 2020 May 14. doi: 10.1038/s41586-020-2342-5.*
627 *Online ahead of print.PMID: 32408338.*
628 Sterlin, D., A. Mathian, M. Miyara, A. Mohr, F. Anna, L. Claër, P. Quentric, J. Fadlallah, P. Ghillani,
629 C. Gunn, R. Hockett, S. Mudumba, A. Guihot, C. Luyt, J. Mayaux, A. Beurton, S. Fourati, J.
630 Lacorte, H. Yssel, C. Parizot, K. Dorgham, P. Charneau, Z. Amoura, and G. Gorochov. IgA
631 dominates the early neutralizing antibody response to SARS-CoV-2.
632 https://www.medrxiv.org/content/10.1101/2020.06.10.20126532v1:
633 Vabret, N., G.J. Britton, C. Gruber, S. Hegde, J. Kim, M. Kuksin, R. Levantovsky, L. Malle, A.
634 Moreira, M.D. Park, L. Pia, E. Risson, M. Saffern, B. Salome, M. Esai Selvan, M.P. Spindler,
635 J. Tan, V. van der Heide, J.K. Gregory, K. Alexandropoulos, N. Bhardwaj, B.D. Brown, B.
636 Greenbaum, Z.H. Gumus, D. Homann, A. Horowitz, A.O. Kamphorst, M.A. Curotto de
637 Lafaille, S. Mehandru, M. Merad, R.M. Samstein, and P. Sinai Immunology Review. 2020.
638 Immunology of COVID-19: Current State of the Science. *Immunity* 52:910-941.

639 Walls, A.C., Y.J. Park, M.A. Tortorici, A. Wall, A.T. McGuire, and D. Veesler. 2020. Structure,
640 Function, and Antigenicity of the SARS-CoV-2 Spike Glycoprotein. *Cell* 181:281-292 e286.
641 Wan, Y., J. Shang, S. Sun, W. Tai, J. Chen, Q. Geng, L. He, Y. Chen, J. Wu, Z. Shi, Y. Zhou, L. Du,
642 and F. Li. 2020. Molecular Mechanism for Antibody-Dependent Enhancement of Coronavirus
643 Entry. *J Virol* 94:
644 Wang, Q., Y. Qiu, J.Y. Li, Z.J. Zhou, C.H. Liao, and X.Y. Ge. 2020. A Unique Protease Cleavage Site
645 Predicted in the Spike Protein of the Novel Pneumonia Coronavirus (2019-nCoV) Potentially
646 Related to Viral Transmissibility. *Virol Sin. 2020 Jun;35(3):337-339. doi: 10.1007/s12250-*
647 *020-00212-7. Epub 2020 Mar 20.*
648 Yu, J., L.H. Tostanoski, L. Peter, N.B. Mercado, K. McMahan, S.H. Mahrokhian, J.P. Nkolola, J. Liu,
649 Z. Li, A. Chandrashekar, D.R. Martinez, C. Loos, C. Atyeo, S. Fischinger, J.S. Burke, M.D.
650 Slein, Y. Chen, A. Zuiani, N.L. FJ, M. Travers, S. Habibi, L. Pessaint, A. Van Ry, K. Blade, R.
651 Brown, A. Cook, B. Finneyfrock, A. Dodson, E. Teow, J. Velasco, R. Zahn, F. Wegmann, E.A.
652 Bondzie, G. Dagotto, M.S. Gebre, X. He, C. Jacob-Dolan, M. Kirilova, N. Kordana, Z. Lin,
653 L.F. Maxfield, F. Nampanya, R. Nityanandam, J.D. Ventura, H. Wan, Y. Cai, B. Chen, A.G.
654 Schmidt, D.R. Wesemann, R.S. Baric, G. Alter, H. Andersen, M.G. Lewis, and D.H. Barouch.
655 2020. DNA vaccine protection against SARS-CoV-2 in rhesus macaques. *Science. 2020 May*
656 *20;eabc6284. doi: 10.1126/science.abc6284. PMID: 32434945.*
657 Zennou, V., C. Petit, D. Guetard, U. Nerhbass, L. Montagnier, and P. Charneau. 2000. HIV-1 genome
658 nuclear import is mediated by a central DNA flap. *Cell* 101:173-185.
659 Zhao, J., K. Li, C. Wohlford-Lenane, S.S. Agnihothram, C. Fett, J. Zhao, M.J. Gale, Jr., R.S. Baric, L.
660 Enjuanes, T. Gallagher, P.B. McCray, Jr., and S. Perlman. 2014. Rapid generation of a mouse
661 model for Middle East respiratory syndrome. *Proc Natl Acad Sci U S A* 111:4970-4975.
662 Zhu, F.C., Y.H. Li, X.H. Guan, L.H. Hou, W.J. Wang, J.X. Li, S.P. Wu, B.S. Wang, Z. Wang, L. Wang,
663 S.Y. Jia, H.D. Jiang, L. Wang, T. Jiang, Y. Hu, J.B. Gou, S.B. Xu, J.J. Xu, X.W. Wang, W.
664 Wang, and W. Chen. 2020. Safety, tolerability, and immunogenicity of a recombinant
665 adenovirus type-5 vectored COVID-19 vaccine: a dose-escalation, open-label, non-
666 randomised, first-in-human trial. *Lancet. 2020 Jun 13;395(10240):1845-1854. doi:*
667 *10.1016/S0140-6736(20)31208-3. Epub 2020 May 22. P.*

668

669

670 **Figure Legend**

671 **Figure 1. Induction of S_{CoV-2}-specific antibody responses by LV. (A)** Schematic representation
672 of 3 forms of S_{CoV-2} protein (S_{FL}, S1-S2 and S1) encoded by LV injected to mice. RBD, S1/S2 and S2'
673 cleavage sites, Fusion Peptide (FP), TransMembrane (TM) and short internal tail (T) are indicated. **(B)**
674 Dynamic of S_{CoV-2}-specific Ab response following LV immunization. C57BL/6 mice (*n* = 4/group)
675 were injected i.p. with 1×10^7 TU of LV::S_{FL}, LV::S1-S2, LV::S1 or, LV::GFP as a negative control.
676 Sera were collected at 1, 3, 4 and 6 weeks post immunization. Anti-S_{CoV-2} IgG responses were evaluated
677 by ELISA and expressed as mean endpoint dilution titers. **(C)** Neutralization capacity of S_{CoV-2}-specific
678 antibodies induced by LV::S_{FL} immunization. Mouse sera were evaluated in a sero-neutralization assay
679 to determine 50% effective concentration (EC50) neutralizing titers. (D) Correlation between the Ab
680 titers and neutralization activity in various experimental groups. NS: not significant. **(E)** Head-to-head
681 comparison at a 1:40 dilution between mouse sera taken at weeks 3 or 4 after immunization and a
682 cohort of mildly symptomatic people living in Crépy en Valois, Ile de France. These patients did not
683 seek medical attention and recovered from COVID-19. Results are expressed as Mean ± SEM
684 percentages of inhibition of luciferase activity.

685 **Figure 2. Induction of T-cell responses by LV::S_{FL}.** Naive C57BL/6 mice (*n* = 5) were immunized
686 i.p. with 1×10^7 TU of LV::S_{FL}. **(A)** Splenocytes collected 2 weeks later were subjected to an IFN-γ
687 ELISPOT using pools of peptides spanning the entire S_{CoV-2} (1-1273 a.a.). SFC = Spot-Forming Cells.
688 **(B)** Deconvolution of the peptide pools by intracellular IFN-γ staining in 5 individual mice. IFN-γ-
689 secreting $CD4^+$ or $CD8^+$ T cells were detected after stimulation with individual peptides from positive
690 pools. Percentages of S_{CoV2}-specific IFN-γ-producing cells versus total $CD4^+$ or $CD8^+$ T cells are
691 shown as color map. ND = not done.

692 **Figure 3. In vivo transduction of mouse respiratory tract cells by an Ad5::hACE2**
693 **pretreatment, allowing permissibility to SARS-CoV-2 replication. (A)** Detection of hACE2
694 expression by RT-PCR in HEK293 T cells transduced with Ad5::hACE2 at 2 days post transduction.
695 **(B)** hACE2 protein detection by Western Blot in lung cell extracts recovered at day 4 after i.n.
696 instillation of Ad5::hACE2 or empty Ad5 to C57BL/6 mice (*n* = 2/group). **(C)** GFP expression in the
697 lung cells prepared at day 4 after i.n. instillation of Ad5::GFP or PBS into C57BL/6 mice, as assessed
698 by flow cytometry in the $CD45^+$ hematopoietic or $EpCam^+$ epithelial cells. **(D)** Lung viral loads in mice
699 pretreated with Ad5::hACE2, control empty Ad5 or PBS followed by i.n. inoculation of 1×10^5 $TCID_{50}$
700 of SARS-CoV-2 4 days later. Viral loads quantification by qPCR in the lung homogenates at 2, 4 or 7
701 dpi. Limit of detection is shown by a brown line **(E)** Percentages of $CD45^+$ cells, and **(F)** SARS-CoV-
702 2 viral loads in the lungs at day 4 after i.n. instillation of various doses of Ad5::hACE2.

703 **Figure 4. Protective potential of LV::S_{FL} immunization against SARS-CoV-2 in mice. (A)** Time
704 line of vaccination by a single injection of LV followed by Ad5::hACE2 pretreatment and SARS-CoV-

705 2 challenge. **(B)** Lung viral loads in unvaccinated mice, LV::S_{FL}- or sham-immunized mice, at 3 dpi
706 post challenge. **(C)** Time line of the prime-boost strategy based on LV, followed by Ad5::hACE2
707 pretreatment and SARS-CoV-2 challenge. **(D)** Titers of S_{CoV-2}-specific IgG, able to bind to S_{CoV-2}, as
708 quantitated by ELISA in the sera of C57BL/6 mice primed i.p. at week 0 and boosted i.p. or i.n. at
709 week 3. Titers are determined as mean endpoint dilution. *** $P<0.001$; **** $P<0.0001$. ns, not
710 significant. **(E)**. Lung viral loads at 3 dpi in mice primed (i.p.) and boosted (i.p. or i.n.) with LV::S_{FL}.
711 Sham-vaccinated received an empty LV. Statistical significance of the differences in the viral loads was
712 evaluated by two tailed unpaired t test; * = $p<0.0139$, *** = $p<0.0088$.

713 **Figure 5. Inflammation mediators in the lungs of unvaccinated or vaccinated and protected**
714 **mice. (A)** Gating strategy applied to total lung cells to quantitate the key innate immune subsets. **(B)**
715 Percentages of each innate immune subset versus total lung $CD45^+$ cells at 3 dpi in mice sham-
716 vaccinated or vaccinated with LV::S_{FL}, following various prime-boost regimen compared to non-
717 infected (NI) controls which only received PBS. All the mice have been pretreated with Ad5::hACE-
718 2, 4 days prior to SARS-CoV-2 inoculation. **(C)** Relative $\log_2$ fold change in cytokines and chemokines
719 expression of mice sham-vaccinated or vaccinated with LV::S_{FL}, following various prime-boost
720 regimen at 3 dpi.

721 **Figure 6. LV::S_{FL} immunization against SARS-CoV-2 in hamsters. (A)** Time line of the LV::S_{FL}
722 prime-boost/target immunization regimen and SARS-CoV-2 challenge in hamsters. (n = 6/group).
723 Sham-vaccinated received an empty LV. **(B)** Dynamic of S_{CoV-2}-specific Ab response following LV
724 immunization. Sera were collected from sham- or LV-vaccinated hamsters at 3, 5 (pre-boost), and 6
725 (post-boost) weeks after the prime injection. Anti-S_{CoV-2} IgG responses were evaluated by ELISA and
726 expressed as mean endpoint dilution titers. **(C)** Post boost/target EC50 neutralizing titers, determined
727 in the hamsters' sera after boost, and as compared to the sera from a cohort of symptomatic (S), pauci-
728 symptomatic (PS), symptomatic (S) or healthy COVID-19 contacts (H) humans **(D)** Weight follow-up
729 in hamsters, either sham-vaccinated or vaccinated with diverse doses of LV::S_{FL}.

730 **Figure 7. Protective potential of LV::S_{FL} immunization against SARS-CoV-2 in hamsters.**
731 Animals are those detailed in the Figure 6. **(A)** Lung viral loads at 2 or 4 dpi with SARS-CoV-2 in
732 LV::S_{FL}-vaccinated hamsters. Statistical significance of the differences in the viral loads was evaluated by
733 two tailed unpaired t test; * = $p<0.0402$, **** = $p<0.0001$. **(B)** Relative $\log_2$ fold changes in cytokines
734 and chemokines expression of LV::S_{FL}-vaccinated and protected hamsters versus unprotected sham-
735 vaccinated individuals, as determined at 4 dpi by qRT-PCR in the total lung homogenates. And
736 normalized versus untreated controls. Statistical significance of the differences in cytokines and
737 chemokines level was evaluated by one-way ANOVA; * = $p<0.05$, ** = $p<0.01$.

738

739

740 **Author Contribution**

741 Study concept and design: MWK, MB, FA, AM, NE, LM, PC, acquisition of data: MWK, MB, PA,
742 JL, KN, BV, PS, FA, AM, LM, construction and production of LV and technical support: PA, FM,
743 AN, FN, CB, PS, analysis and interpretation of data: MWK, MB, PA, JL, KN, FA, AM, NE, LM, PC,
744 recombinant S proteins: HM, drafting of the manuscript: MWK, MB, LM.

745

746 **Declaration of Interests**

747 PC is the founder and CSO of TheraVectys. Other authors declare no competing interests.

748

749 **Acknowledgments**

750 The authors are grateful to Cyril Planchais for the preparation of recombinant Tri-S, S1 and RBD
751 proteins and Damien Batalie for technical assistance in determination of viral loads.

752 This work is also supported by grants from Institut Pasteur, TheraVectys and Agence Nationale de
753 la Recherche (ANR) HuMoCID.

Figure 1

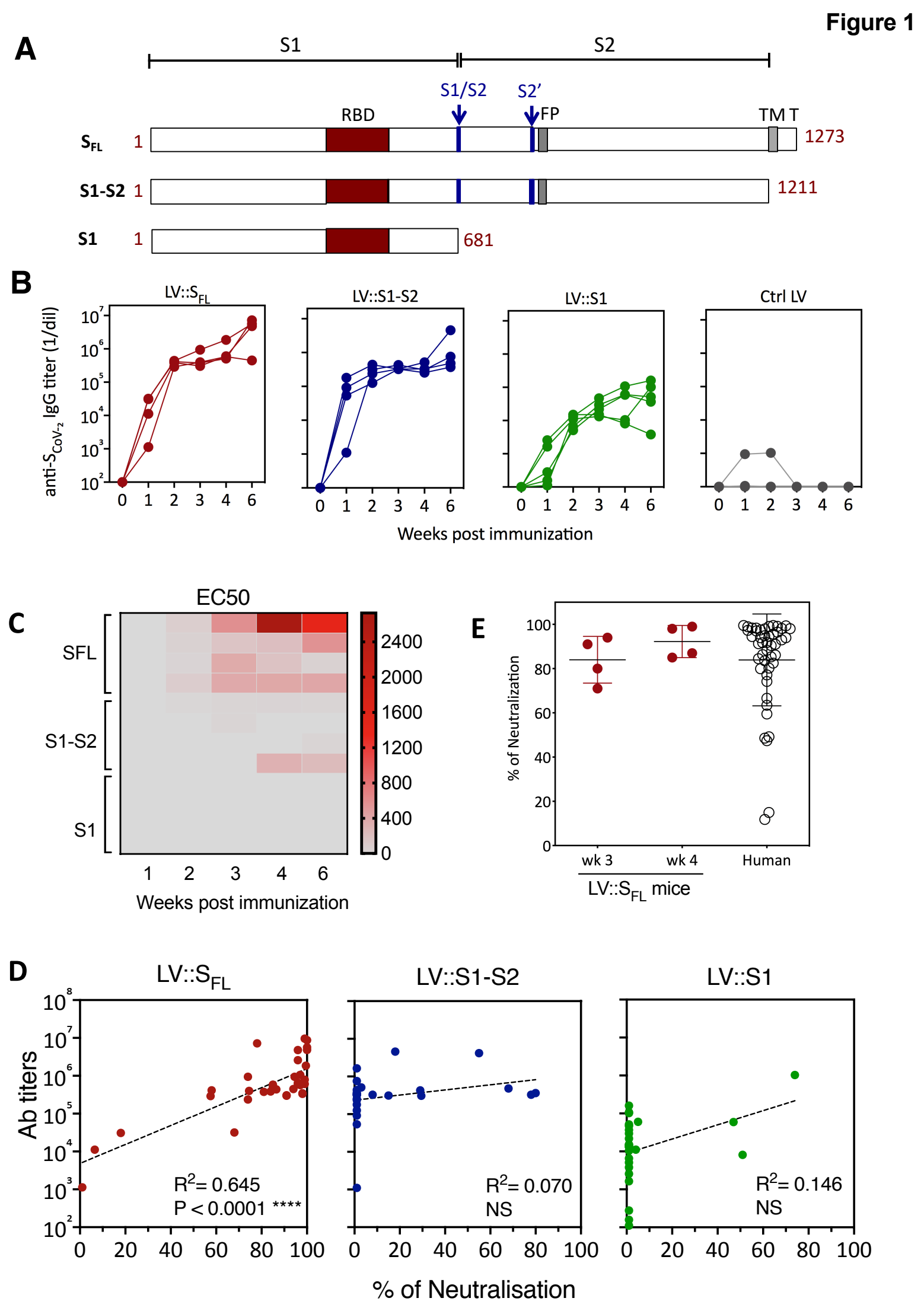
A
S1
S2
S1/S2
S2'
RBD
FP
TM T
S_FL
1
1273
S1-S2
1
1211
S1
1
681
B
LV::S_FL
LV::S1-S2
LV::S1
Ctrl LV
anti-S_CoV-2 IgG titer (1/dil)
Weeks post immunization
C
EC50
SFL
S1-S2
S1
Weeks post immunization
E
% of Neutralization
wk 3
wk 4
Human
LV::S_FL mice
D
LV::S_FL
LV::S1-S2
LV::S1
Ab titers
R2= 0.645
P < 0.0001 ****
R2= 0.070
NS
R2= 0.146
NS
% of Neutralisation

Figure 2

A

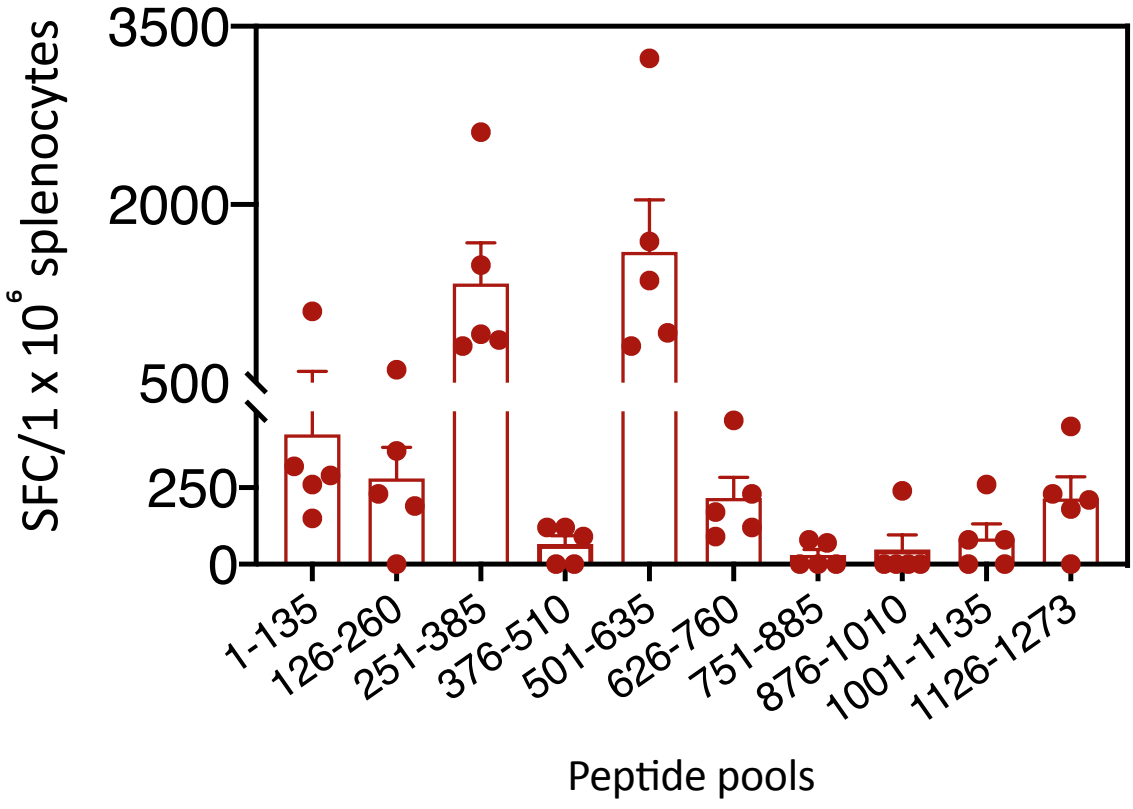
SFC/1 x 10^6 splenocytes
3500
2000
500
250
0
1-135
126-260
251-385
376-510
501-635
626-760
751-885
876-1010
1001-1135
1126-1273
Peptide pools

B

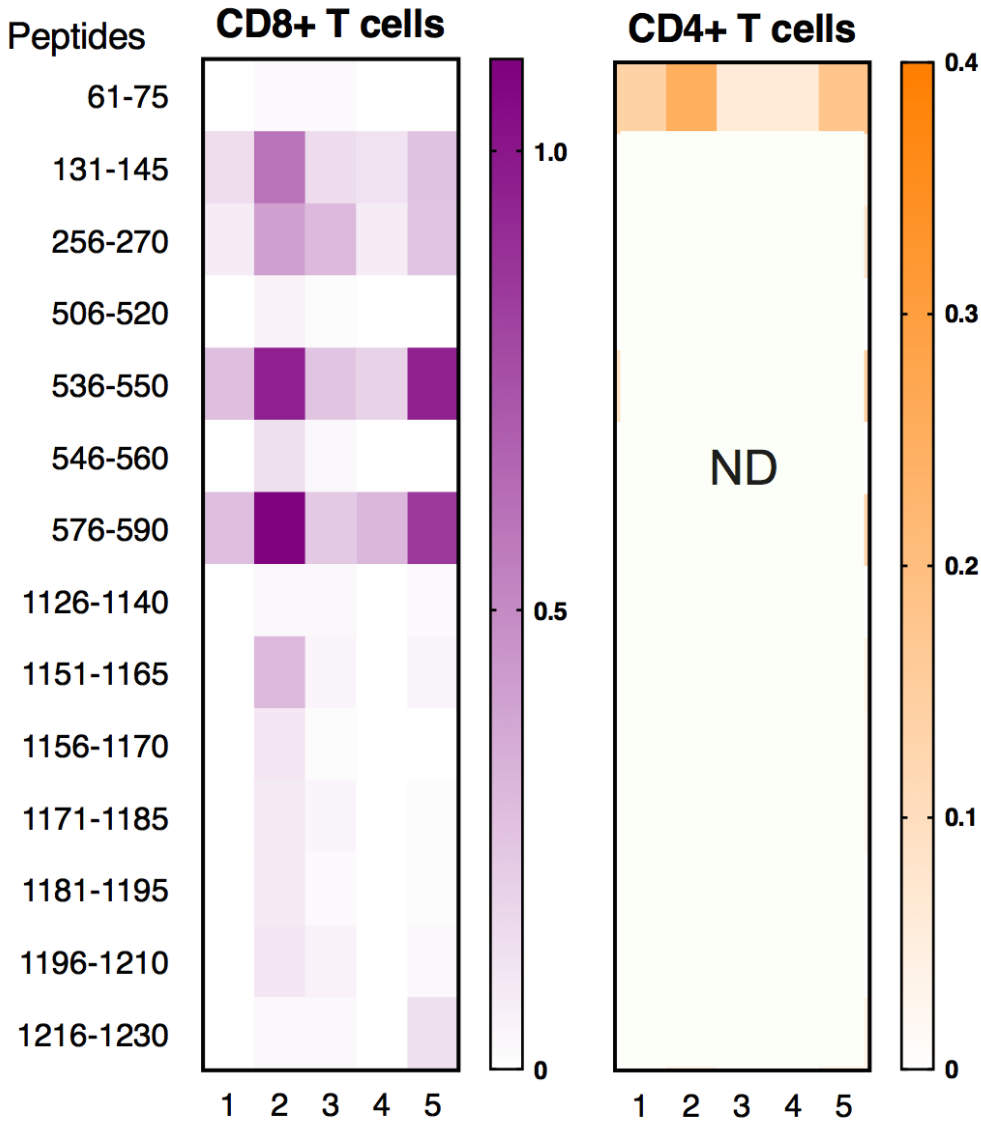
Peptides
CD8+ T cells
CD4+ T cells
61-75
131-145
256-270
506-520
536-550
546-560
576-590
1126-1140
1151-1165
1156-1170
1171-1185
1181-1195
1196-1210
1216-1230
1 2 3 4 5
1.0
0.5
0
ND
0.4
0.3
0.2
0.1
0

Figure 3

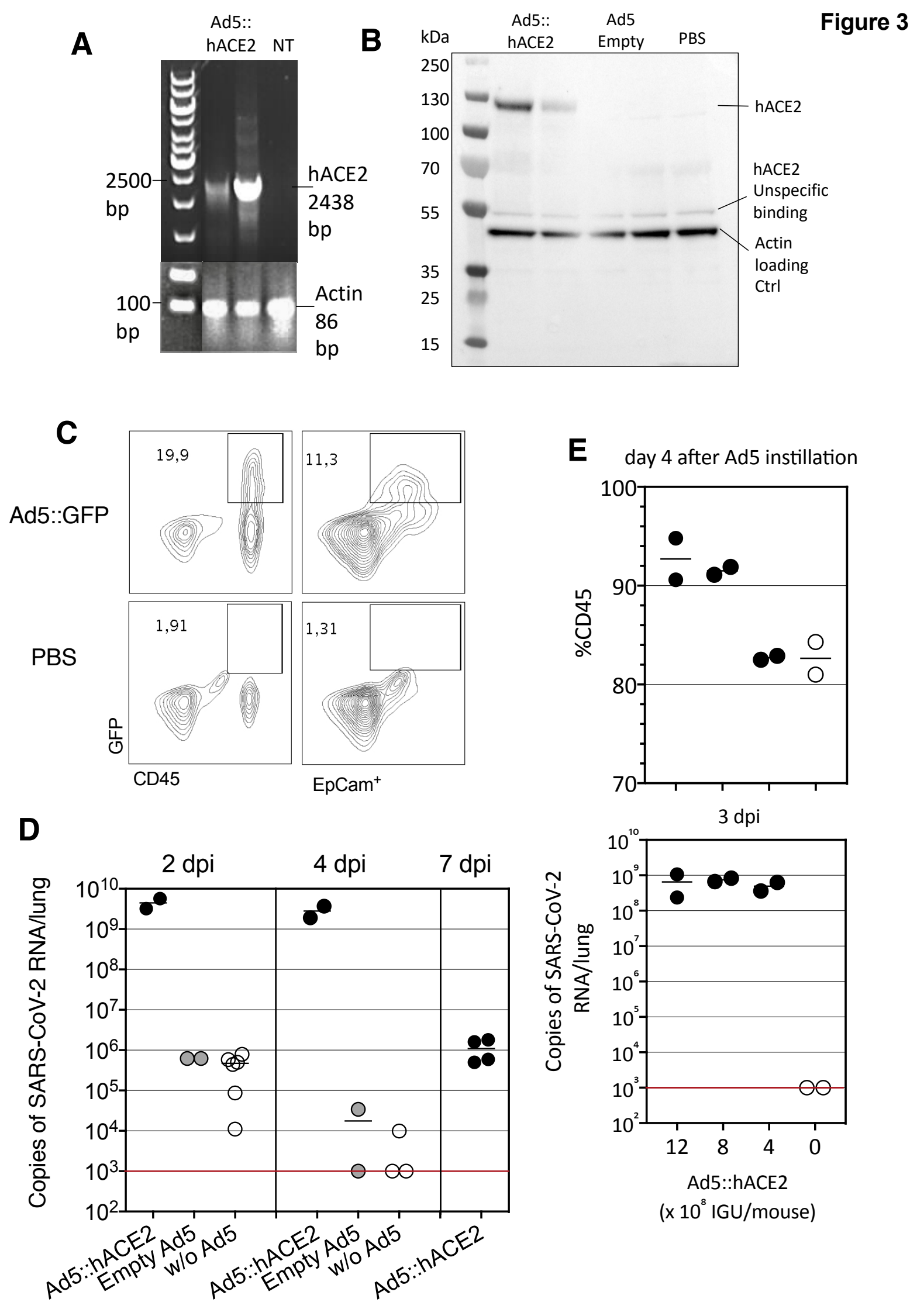
A
Ad5::
hACE2
NT
2500
bp
hACE2
2438
bp
100
bp
Actin
86
bp
B
kDa
Ad5::
hACE2
Ad5
Empty
PBS
250
130
100
70
55
35
25
15
hACE2
hACE2
Unspecific
binding
Actin
loading
Ctrl
C
Ad5::GFP
PBS
19,9
11,3
1,91
1,31
GFP
CD45
EpCam+
E
day 4 after Ad5 instillation
%CD45
100
90
80
70
3 dpi
Copies of SARS-CoV-2
RNA/lung
12
8
4
0
Ad5::hACE2
(x 10^8 IGU/mouse)
D
2 dpi
4 dpi
7 dpi
Copies of SARS-CoV-2 RNA/lung
Ad5::hACE2
Empty Ad5
w/o Ad5
Ad5::hACE2
Empty Ad5
w/o Ad5
Ad5::hACE2

Figure 4

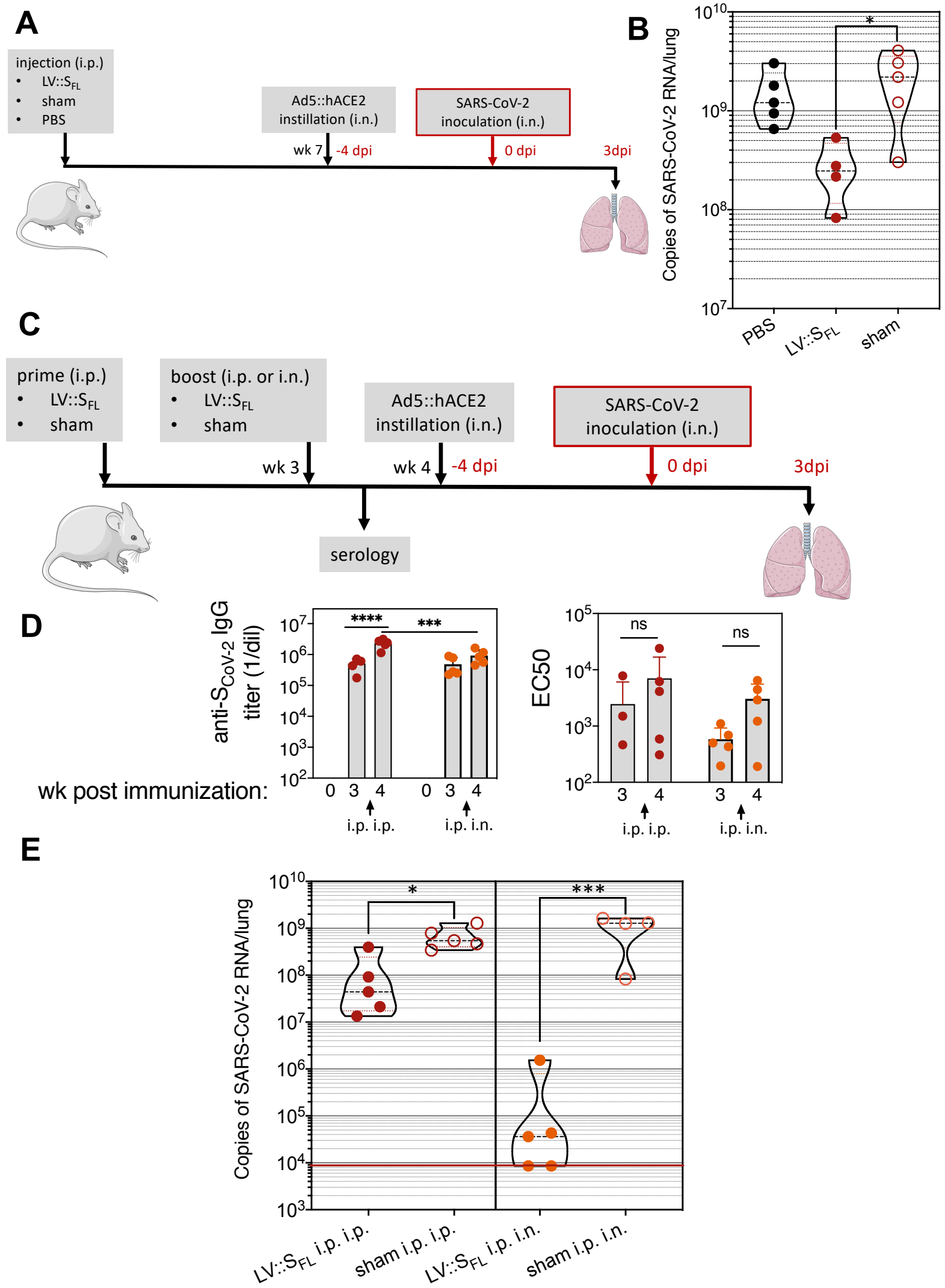
A
injection (i.p.)
• LV::S$_{FL}$
• sham
• PBS
Ad5::hACE2 instillation (i.n.)
SARS-CoV-2 inoculation (i.n.)
wk 7
-4 dpi
0 dpi
3dpi
B
Copies of SARS-CoV-2 RNA/lung
PBS
LV::S$_{FL}$
sham
C
prime (i.p.)
• LV::S$_{FL}$
• sham
boost (i.p. or i.n.)
• LV::S$_{FL}$
• sham
Ad5::hACE2 instillation (i.n.)
SARS-CoV-2 inoculation (i.n.)
wk 3
wk 4
-4 dpi
0 dpi
3dpi
serology
D
anti-S$_{CoV-2}$ IgG titer (1/dil)
EC50
wk post immunization:
i.p. i.p.
i.p. i.n.
ns
E
Copies of SARS-CoV-2 RNA/lung
LV::S$_{FL}$ i.p. i.p.
sham i.p. i.p.
LV::S$_{FL}$ i.p. i.n.
sham i.p. i.n.

Figure 5

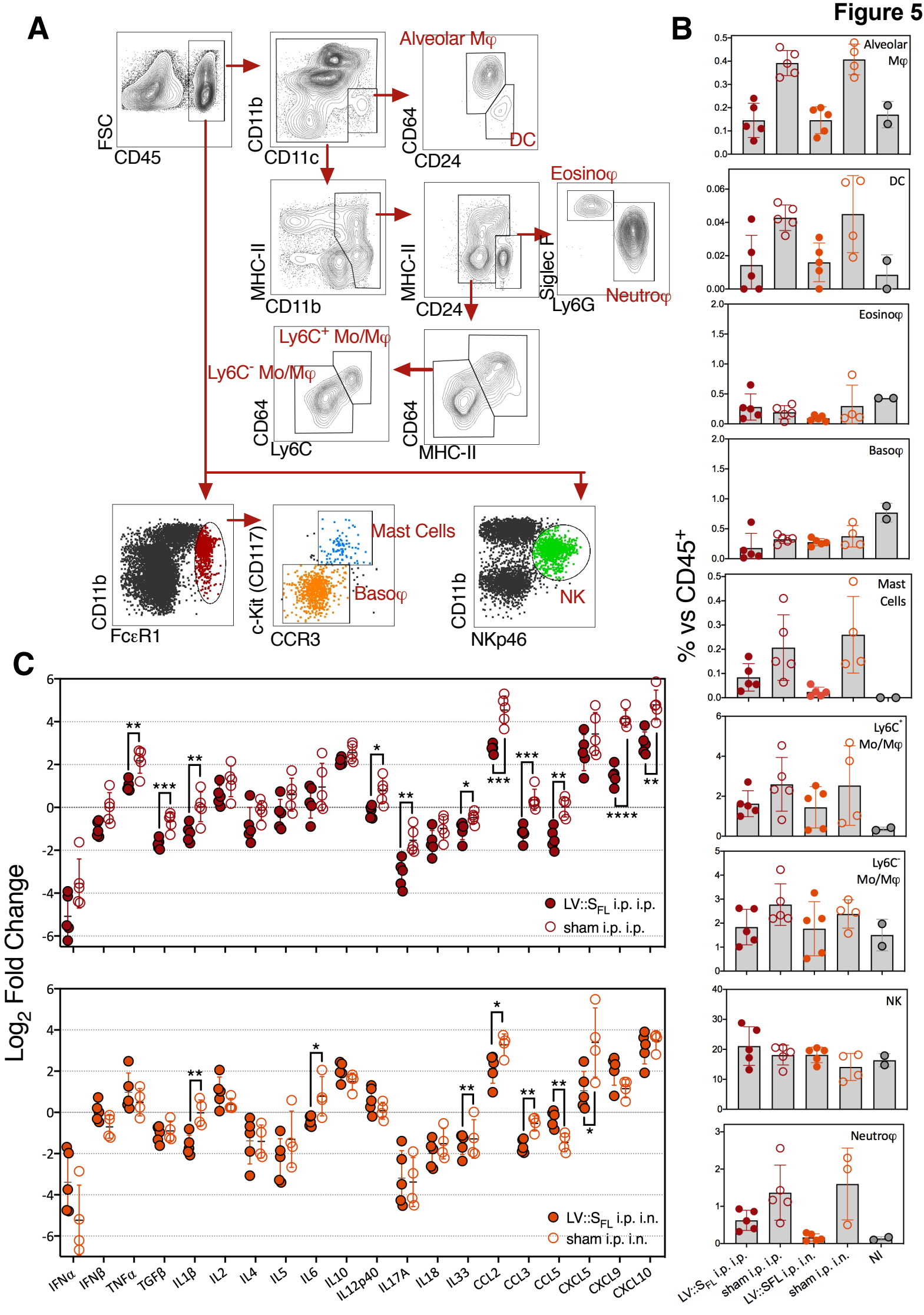
A
FSC
CD45
CD11b
CD11c
Alveolar Mφ
CD64
CD24
DC
MHC-II
CD11b
MHC-II
CD24
Eosinoφ
Siglec F
Ly6G
Neutroφ
Ly6C+ Mo/Mφ
Ly6C- Mo/Mφ
CD64
Ly6C
CD64
MHC-II
CD11b
FcεR1
c-Kit (CD117)
CCR3
Mast Cells
Basoφ
CD11b
NKp46
NK
B
% vs CD45+
Alveolar Mφ
DC
Eosinoφ
Basoφ
Mast Cells
Ly6C+ Mo/Mφ
Ly6C- Mo/Mφ
NK
Neutroφ
LV::SFL i.p. i.p.
sham i.p. i.p.
LV::SFL i.p. i.n.
sham i.p. i.n.
NI
C
Log2 Fold Change
LV::SFL i.p. i.p.
sham i.p. i.p.
LV::SFL i.p. i.n.
sham i.p. i.n.
IFNα
IFNβ
TNFα
TGFβ
IL1β
IL2
IL4
IL5
IL6
IL10
IL12p40
IL17A
IL18
IL33
CCL2
CCL3
CCL5
CXCL5
CXCL9
CXCL10

Figure 6

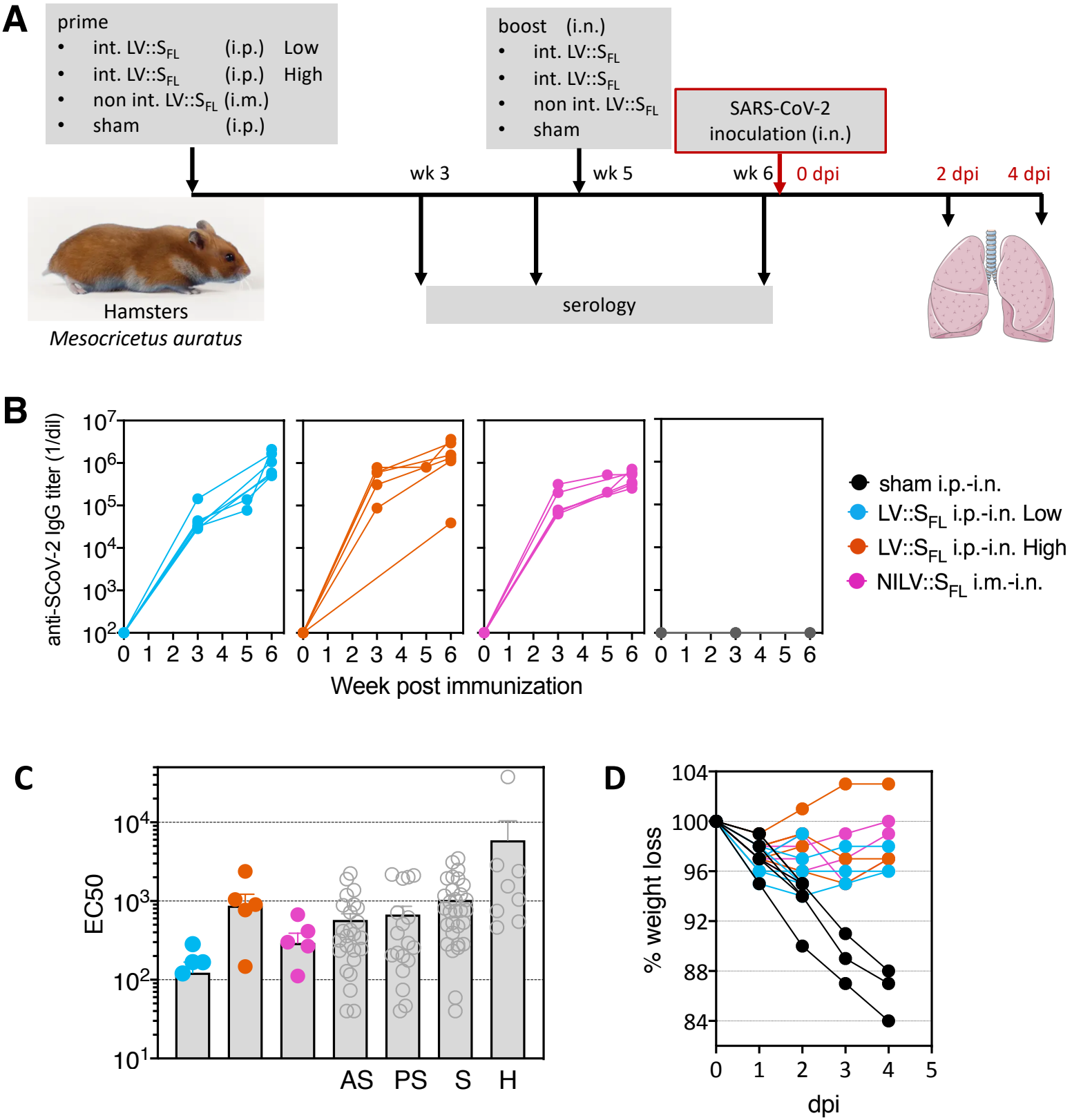
A
prime
int. LV::S_FL (i.p.) Low
int. LV::S_FL (i.p.) High
non int. LV::S_FL (i.m.)
sham (i.p.)
boost (i.n.)
int. LV::S_FL
int. LV::S_FL
non int. LV::S_FL
sham
SARS-CoV-2 inoculation (i.n.)
wk 3
wk 5
wk 6
0 dpi
2 dpi
4 dpi
Hamsters
Mesocricetus auratus
serology
B
anti-SCoV-2 IgG titer (1/dil)
Week post immunization
sham i.p.-i.n.
LV::S_FL i.p.-i.n. Low
LV::S_FL i.p.-i.n. High
NILV::S_FL i.m.-i.n.
C
EC50
AS
PS
S
H
D
% weight loss
dpi

Figure 7

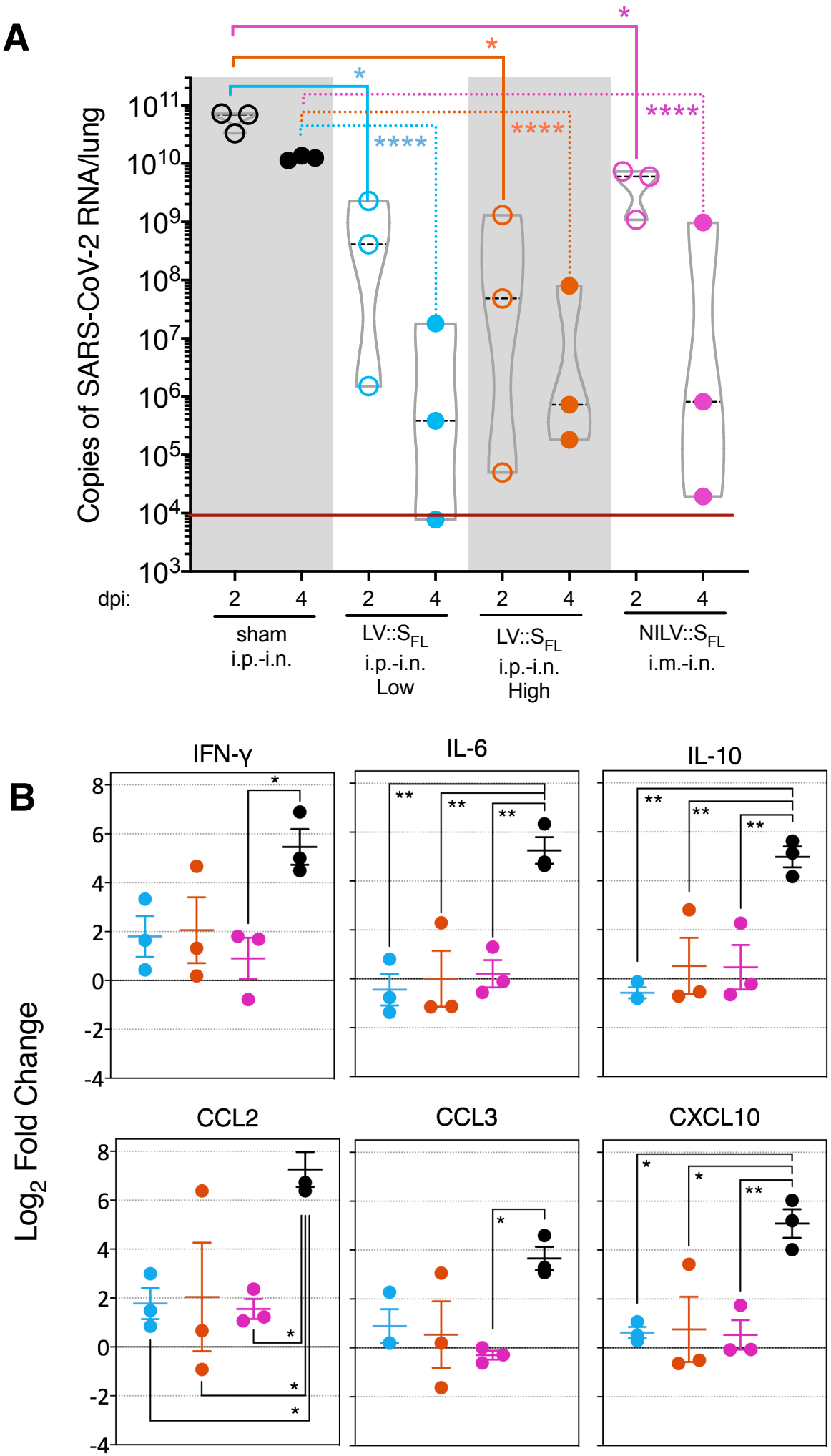
A
Copies of SARS-CoV-2 RNA/lung
10^{11}
10^{10}
10^{9}
10^{8}
10^{7}
10^{6}
10^{5}
10^{4}
10^{3}
dpi:
2
4
sham i.p.-i.n.
LV::S_{FL} i.p.-i.n. Low
LV::S_{FL} i.p.-i.n. High
NILV::S_{FL} i.m.-i.n.
B
IFN-γ
IL-6
IL-10
CCL2
CCL3
CXCL10
Log_2 Fold Change